Dalton Transactions

ROYAL SOCIETY OF CHEMISTRY

PAPER

View Article Online
View Journal | View Issue

Cite this: *Dalton Trans.*, 2022, **51**, 6718

Experimental and computational tuning of metalla-N-heterocyclic carbenes at palladium(II) and platinum(II) centers†

Maria V. Kashina, [a] Konstantin V. Luzyanin, *[b] Eugene A. Katlenok, [a] Alexander S. Novikov[a] and Mikhail A. Kinzhalov *[a]

Palladium(II) and platinum(II) complexes featuring metalla-N-heterocyclic carbenes (**7–12**) were synthesised *via* metal-mediated coupling between equimolar *cis*-[$MCl_2(CNR)_2$] (R = 2,6-$Me_2C_6H_3$ (Xyl), 2,4,6-$Me_3C_6H_3$ (Mes)) and 2-aminopyridine or 2-aminopyrazine. Thiocyanate complexes **13–18** with two thiocyanate ligands were obtained through the ligand exchange in the parent compounds **7–12** with NH_4CNS in acetone/CH_2Cl_2. Complexes **7–18** were isolated and characterised by HRESI$^+$-MS, IR, ^{1}H and $^{13}C\{^1H\}$ NMR spectroscopy and single-crystal X-ray diffraction (in the case of **11**, **16**, and **18**). The UV-vis properties of **7–18** and the electrochemical properties of **7–12** were also evaluated. To study the electronic structure and bonding nature in the new compounds, the quantum theory of atoms in molecules (QTAIM) and Mayer bond order analysis together with the extended transition state with the natural orbitals for chemical valence (ETS-NOCV) method, were used. X-ray diffraction studies and theoretical considerations indicate that the thiocyanate derivatives **16** and **18** form supramolecular dimers by two symmetrical pairs $M^1\cdots C^5$ and $S^1\cdots C^2$ with short intermolecular contacts between an electron-rich M^{II}-center and thiocyanate ligand on the one side and the electron-poor π-system of an azaheterocyclic ring on the other side. Representative carbenes **8**, **11** and **12** were evaluated as photocatalysts for the hydrosilylation of diphenylacetylene with triethylsilane giving 1,2-(diphenylvinyl)triethylsilane in 98% yield under visible light irradiation (blue light, 445 nm).

Received 25th January 2022,
Accepted 14th March 2022

DOI: 10.1039/d2dt00252c

rsc.li/dalton

Introduction

Transition metal complexes with heteroatom-stabilised carbenes, *i.e.* N-heterocyclic carbenes (NHCs)[1] and acyclic diaminocarbenes (ADCs),[2] underpin a broad range of applications in the catalysis of organic processes;[1a,2a,3] they are studied as emissive materials in optoelectronics[4] and potential anticancer drugs.[2a,5] The ligand properties of diaminocarbenes are manifested through the formation of the M–$C_{carbene}$ σ-bond by transferring a pair of nonbonding electrons from the nucleophilic σ-orbital of the carbene carbon atom to the metal atom M. At the same time, the formation of a π-bond is also possible as a result of the interaction of a vacant electron-deficient pπ-orbital of a carbene carbon atom with a metal, whose orbital symmetry is suitable. The diaminocarbene ligand is usually an effective σ-donor and a weak π-acceptor, which is reflected in the catalytic and photophysical properties of the respective metal complexes. Tuning of the electron-donor capacity of diaminocarbenes, which is crucial for the success of their target applications, has been mainly accomplished by varying the substituents on the nitrogen atoms or the modification of the heterocyclic skeleton (Fig. 1A). It was shown that NHC complexes containing a metal atom within the NHC skeleton, named metalla-N-heterocyclic carbenes (MNHCs),[6] exhibit a stronger electron-donor character by comparison with classical imidazole-2-ylidenes.[7] In pursuit of our ongoing project on the chemistry of diaminocarbenes,[3d,e,8] we have reported that platinum(II)–MNHC species (Fig. 1B) work as self-photosensitising transition-metal photocatalysts for the hydrosilylation of alkynes under visible light.[9] In this catalytic reaction the platinum(II)–MNHC catalyst has a dual function: it serves as a light-absorbing species and a transition metal catalyst enabling the catalytic process.

Additional strategies for fine-tuning the properties of complexes of this type are linked to (i) the modification of the structure of the azaheterocyclic ring (highlighted with a yellow

[a]St Petersburg University, 7/9 Universitetskaya Nab., Saint Petersburg 199034, Russian Federation. E-mail: m.kinzhalov@spbu.ru
[b]Department of Chemistry, University of Liverpool, Crown Street, Liverpool L69 7ZD, UK. E-mail: konstantin.luzyanin@liverpool.ac.uk

† Electronic supplementary information (ESI) available. CCDC 2133432, 2133433 and 2133435. For ESI and crystallographic data in CIF or other electronic format see DOI: http://doi.org/10.1039/d2dt00252c

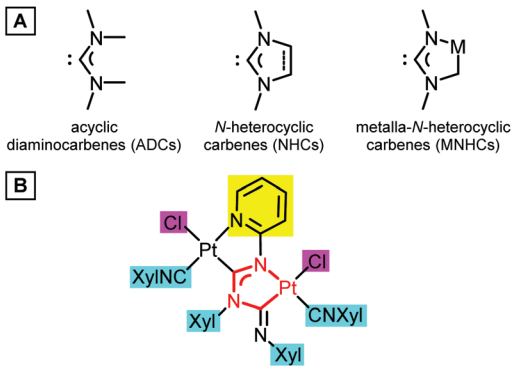

Fig. 1 (A) Examples of cyclic, N-heterocyclic and metalla-N-heterocyclic diaminocarbenes. (B) The platinum(II)–MNHC catalyst exhibiting photocatalytic properties under visible light irradiation.

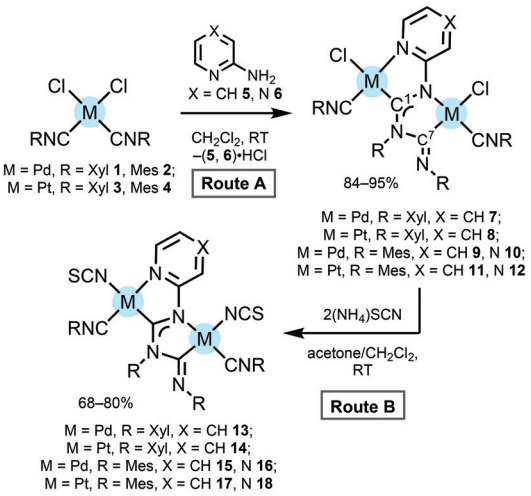

Scheme 1 Preparation of 7–18.

rectangle), (ii) substitution in the aryl rings (highlighted with a cyan rectangle), and (iii) the replacement of the anionic ligands at both metal centers (highlighted with a magenta rectangle). An interplay of these will define the application of the complex thus designed towards a specific goal.

The scenario of this work was as follows. We started by the preparation of a series of palladium(II)– and platinum(II)–MNHC complexes *via* the metal-mediated coupling of isocyanides with various 2-aminoazaheterocycles. The displacement of chlorides with thiocyanates led to the generation of previously unknown diaminocarbene-thiocyanate derivatives. The electronic structure and bonding nature in all new compounds were assessed by using the quantum theory of atoms in molecules (QTAIM), the natural bond orbital (NBO) analysis, and Mayer bond order analysis together with the extended transition state with the natural orbitals for chemical valence (ETS-NOCV) method. Analysis of the frontier molecular orbital character, energy gaps, and UV/vis spectra by density functional theory (DFT) and time-dependent DFT (TD-DFT) approaches provided insights into the excited states involved in the light absorption and electrochemical processes, in turn, related to the potential photocatalytic properties. Finally, we assessed the catalytic properties of the thus prepared carbene complexes in the photocatalytic hydrosilylation of alkynes under visible light irradiation.

Results and discussion

Preparation and characterisation of metalla-N-heterocyclic diaminocarbenes

For this study, a series of Pd^{II} and Pt^{II} MNHC species **7–12** were prepared *via* the nucleophilic addition of 2-aminoazaheterocycles **5** and **6** to metal-bound isocyanides in *cis*-$[MCl_2(CNR)_2]$ (**1–4**, M = Pd, Pt). The reaction of **1–4** and azaheterocycles **5**, **6** proceeds in CH_2Cl_2 at RT for *ca.* 1 d and the subsequent workup provided the binuclear diaminocarbene species **7–12** in good (84–95%) isolated yields (Scheme 1, Route **A**). This process occurs *via* the intermediate generation of the corresponding mononuclear M-ADC species and its nucleophilic addition to the unreacted isocyanide material facilitated by the deprotonation of the M-ADC intermediate by an excess of the aminoazaheterocycle used.[9,10]

MNHC complexes **7–12** are yellow solids stable in the 20–80 °C temperature range. New complexes **9–12** were characterised by elemental analyses (C, H, and N), accurate-mass ESI^+-MS, IR, 1D (^1H, $^{13}C\{^1H\}$, and $^{195}Pt\{^1H\}$) NMR and 2D (^1H,^{13}C-HSQC and ^1H,^{13}C-HMBC) NMR spectroscopy (see the Experimental section for more details), while the authenticity of the known species **7** and **8** was confirmed by ^1H NMR spectroscopy.[9,10] The intense absorption bands at 1619–1667 cm^{-1} in the FTIR spectra of **7–12** were assigned to $\nu(C_{carbene}–N)$ of the NCN moiety. For **7–12**, the important ^{13}C resonances of the C atoms from two carbene ligands are different and are detected at δ_C 168 and 182 ppm. This evidences that two NCN groups in **7–12** are substantially structurally different; one of them (having the downfield resonance at δ_C 168 ppm and assigned to C^7 carbon) is of the amidine type, whereas another one (having the downfield resonance at δ_C 182 ppm and assigned to C^1 carbon) is of the diaminocarbene type. These δ_C values for diaminocarbene carbon C^1 are downfield relative to those (δ_C 157–159) reported for the series of palladium complexes featuring chelated NHCs, such as bis(imidazolylidene) palladium dichloride complexes,[80] but are some upfield of the δ_C 197–201 range observed for the series of palladium complexes featuring chelating acyclic aminocarbene ligands, *i.e.* $[PdCl\{C(N{=}C(C_6R^2R^3R^4R^5CON)){=}N(H)R^1\}(C{=}NR^1)]$.[11]

The thiocyanate anion NCS^- enables several pathways to alter the properties of the metal centres due to its ambidentate nature, allowing the coordination *via* either S- or N-ends. To the best of our knowledge, only two examples of thiocyanate diaminocarbene complexes, *viz.* nickel(II)–NHC with *N*-coordinated thiocyanate[12] and gold(I)–NHC with S-coordinated thiocyanate,[13] have been reported. Thiocyanate

species demonstrate better donor abilities and increased dipole moment of complex molecules relative to halide analogues which may lead to better catalytic activity of thiocyanate species, *e.g.* in the Kumada–Corriu coupling reaction.[12] In addition, the better donor character of thiocyanate is related to the stabilisation of the HOMOs of the complexes and their red-shifted absorption in the UV-vis spectrum.[14]

The common method for the preparation of thiocyanate complexes from chloride substrates is a metathetic reaction with NaNCS or KSCN in an aqueous or alcohol solution, occasionally aided by $AgNO_3$ to facilitate chloride subtraction.[15] Metathetic reactions of **7–12** with a three-fold excess of NH_4CNS in acetone/CH_2Cl_2 at RT for 24 h afforded yellow bis(*N*-coordinated thiocyanate) complexes **13–18** in good yields (Scheme 1, Route **B**). Owing to the poor solubility of **13–18** in the most common solvents, all **13–18** were characterized in solution by means of HR-MS (ESI^+) and in the solid state by FTIR and solid-state ^{13}C CP/MAS NMR. The structures of **16** and **18** were also elucidated by single-crystal XRD.

Complexes **13–18** gave satisfactory CHN data, which are consistent with the proposed formulae confirming the replacement of both chloride ligands with thiocyanate. The $HRESI^+$-MS spectra of **13–18** exhibit sets of peaks with the characteristic isotopic distribution due to $[M + H]^+$, $[M + Na]^+$ and/or $[M - NCS]^+$ ions. IR spectroscopy was used to identify the coordination modes of thiocyanate in metal thiocyanate complexes.[16] As a general rule, the value of ν(CN) stretching for the thiocyanate of N-bonded complexes lies near 2050 cm^{-1} (strong band) and that of S-bonded complexes is close to 2100 cm^{-1} (weaker band).[16c] The IR spectra of **13–18** measured in KBr revealed two intense absorption bands in the range 2030–2090 cm^{-1} attributed to the ν(CN) stretching of the N-bonded thiocyanate. Additionally, the FTIR spectra of **13–18** displayed strong absorption overlapping bands at *ca.* 2200 cm^{-1} which are also present in the spectra of parent compounds **7–12** and are attributed to the ν(C≡N) of the isocyanide ligands.

UV-Vis absorption properties

All prepared complexes are yellow (**10–18**) or yellowish (**7–9**) solids, which makes them capable of absorbing light in the visible range. UV-vis absorption spectra of **7–18** were measured at ambient temperature in CH_2Cl_2 solution (Fig. 2) and in KBr pellets (Fig. S6 and S7 in the ESI;† UV-vis data for **7–18** are summarised in Table S4 (ESI)).†

Similar to other palladium[17] and platinum[17a,d,18] cyclometallated complexes, the UV-vis spectra of **7–12** contain strong absorption bands below 340 nm [ε = (1.15–3.59) × 10^4 M^{-1} cm^{-1}] assigned to π–π* ligand centred transitions in the xylyl and mesityl moieties (Fig. 2).[19] The wide intense absorption bands in the 340–450 nm range with characteristic molar extinction coefficients [ε = (0.60–1.13) × 10^4 M^{-1} cm^{-1}] can be assigned to mixed ^{1}L′LCT (ligand-to-ligand charge transfer) and ^{1}ILCT (intraligand charge transfer) transitions based on TD-DFT calculations (see the section TD-DFT calculations).

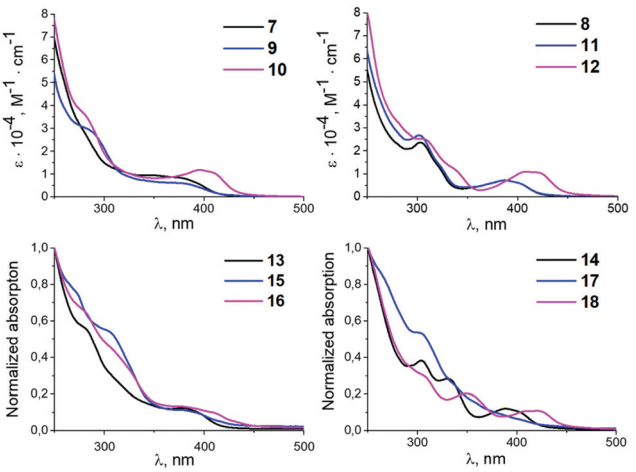

Fig. 2 UV-vis absorption spectra for **7–18** in CH_2Cl_2 at RT (0.03 mM for **7–12** and saturated solutions for **13–18**).

The energy of the ^{1}L′LCT/^{1}ILCT absorption band is affected by the change of the azaheterocyclic fragment.[20] Complexes with pyridine rings **7–9** and **11** show blue-shifted ^{1}L′LCT/^{1}ILCT bands relative to their pyrazine counterparts **10** and **12** (*e.g.* 364–398 nm [ε = (0.60–0.83) × 10^3 M^{-1} cm^{-1}] in **7–9** and **11** *vs.* 402–414 nm [ε = (1.06–1.13) × 10^3 M^{-1} cm^{-1}] in **10** and **12**).

This could be explained by a decrease of the LUMO energy in the case of **10** and **12** with pyrazine species due to the additional intercalation electron negative nitrogen atom in the azaheterocyclic fragment. Variation of the aryl fragment of the CNR or the corresponding diaminocarbene ligands induces no significant changes in the positions of the ^{1}L′LCT/^{1}ILCT bands and only exerts minimal influence on the extinction coefficients (*e.g.* 364–393 nm [ε = (0.64–0.83) × 10^3 M^{-1} cm^{-1}] in **7** and **8** *vs.* 378–414 nm [ε = (0.60–1.13) × 10^3 M^{-1} cm^{-1}] in **9–12**).

The UV-vis spectra of **13–18** demonstrate similar absorption profiles to the spectra of the **7–12** (Fig. 2). Replacing both chloride ligands with thiocyanate ligands leads to minor changes in the absorption spectra. Complexes **7–18** are not fluorescent and/or phosphorescent at RT, and no emission bands were detected.

Frontier molecular orbital analysis

To gain insight into the electronic structures and optical properties of the obtained complexes time-dependent DFT calculations on **7**, **8**, **11**, and **12** were undertaken. The theoretically predicted structures are in good agreement with experimental X-ray structures (Fig. S8 and Table S5 in the ESI†). In general, the computed bond lengths are close to the experimental ones indicating sufficient accuracy of the selected computational protocol.[21] The main difference lies in slight elongation of coordination bonds (by 0.01–0.03 Å) and CN triple bonds (0.03–0.04 Å) in the optimized structures compared to experimental results, due to relaxation of the cyclic metal including systems.

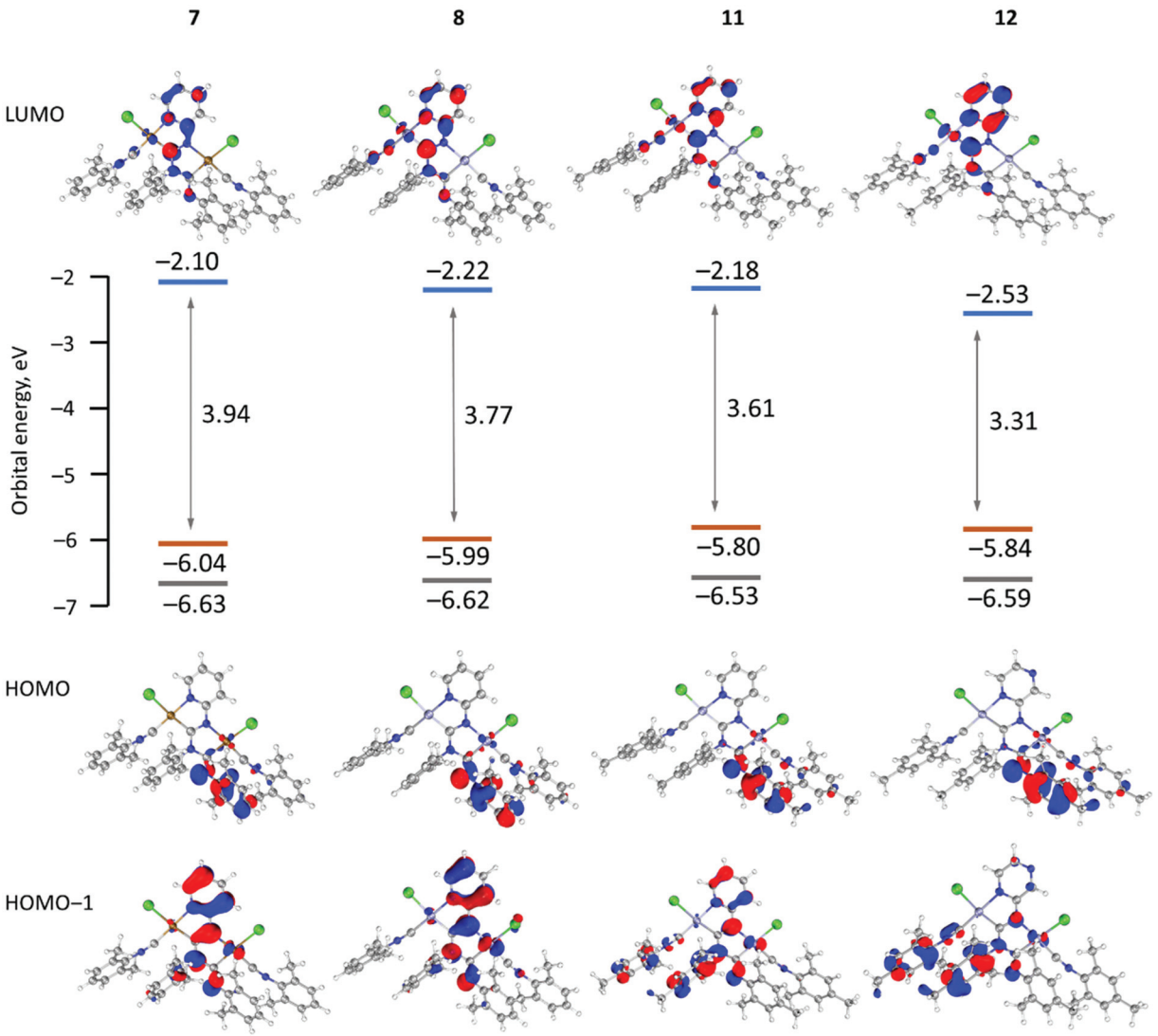

Fig. 3 Calculated molecular orbital energy HOMO–LUMO gaps and surface plots of the HOMO–1, HOMO and LUMO for **7**, **8**, **11** and **12**.

Fig. 3 shows the shape and energy of the frontier molecular orbitals for **7**, **8**, **11**, and **12**, while the FMO compositions are given in Table S8.† In all cases, the highest occupied molecular orbitals (HOMOs) are delocalized by the π molecular orbitals on the aryl ring connected with the exocyclic nitrogen atom of the diaminocarbene species (contribution of aryls >80%), while the contribution of the metal d orbitals is insignificant (<5%). The energies of the HOMOs of **7**, **8**, **11**, and **12** are similar, while the lowest unoccupied molecular orbitals (LUMOs) are localised over the entire diaminocarbene (22–34%) and azaheterocyclic (38–54%) species. The large contribution (12–16%) from the metal d orbitals in the LUMO may be related to the absence of luminescence for **7**–**12** at RT due to the population of a metal-centred state.[22]

The HOMO–LUMO energy difference varies considerably between 3.94 eV (**7**) and 3.31 eV (**12**). The small HOMO–LUMO gap of **12** with pyrazine species comes from the low-lying LUMO which is affected by the additional intercalation of the electron negative nitrogen atom in the azaheterocyclic fragment. There is a correlation between the HOMO–LUMO energy difference and the red-shifted absorption bands determined experimentally for **10** and **12** with pyrazine rings relative to their pyridine counterparts **7**–**9** and **11**.

TD-DFT calculations

TD-DFT calculations were carried out to elucidate the nature of the transitions in the absorbance profile. The TD-DFT calculated UV-vis spectra of all complexes are in good agreement with the experimental ones. The calculated absorption spectra for **7**, **8**, **11**, and **12** are reasonably consistent with the experimental spectral profiles (Fig. S9 and S11†). The absorption band in the 320–450 nm range results from the combination of the most intense transfers appearing at *ca.* 340–360 nm (f *ca.* 0.123–0.156) and *ca.* 393–410 nm (f *ca.* 0.031–0.038) associated correspondingly with the HOMO → LUMO (91–92%) and

HOMO−1 → LUMO (91–94%) transitions (Tables S6 and S7 in the ESI†).

Electrochemical studies

The electrochemical properties of **7**–**12** were examined using cyclic voltammetry (CV) in dichloromethane solution (Fig. 4). Palladium complexes **7**, **9**, and **10** exhibit two irreversible oxidation waves in the ranges of 0.48–0.58 and 0.83–0.85 V, which correspond to the multistep oxidation processes (subsequent oxidation processes are probably assigned to the next step of the oxidation of the mono-oxidized species[23]). Platinum complexes **8**, **11**, and **12** are oxidized at more positive potentials than the corresponding palladium counterparts and the first irreversible oxidation peak was observed in the range of 0.72–0.77 V.

It is worth noting that complexes with mesityl substituent **9**–**12** are oxidized easier than their corresponding analogues **7** and **8** with xylyl substituent. To interpret the electrochemical behaviour of the complexes, quantum-chemical calculations were performed for **7**, **8**, **11**, and **12** and their mono-oxidized forms at the level of the DFT theory. The plot of the spin density calculated for the oxidized forms of **7**, **8**, **11**, and **12** (Fig. 5 and S12†) demonstrates that the first oxidation process could be associated with the oxidation of the aryl fragment connecting to the exocyclic nitrogen atom.

X-Ray diffraction studies of chloride species

Single crystals of **11** were obtained by the slow evaporation of CH_2Cl_2 solution. Crystals of **11** are yellow and possess a low

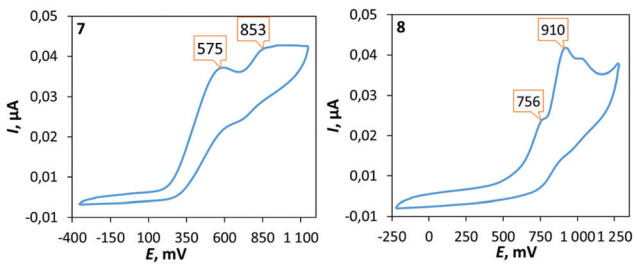

Fig. 4 Cyclic voltammograms of **7** and **8** in CH_2Cl_2 at RT (potentials given in mV *vs.* Fc^+/Fc). Oxidation potentials (mV) of **9**: 483, 833; **10**: 718, 968; **11**: 566, 850; and **12**: 740, 1028.

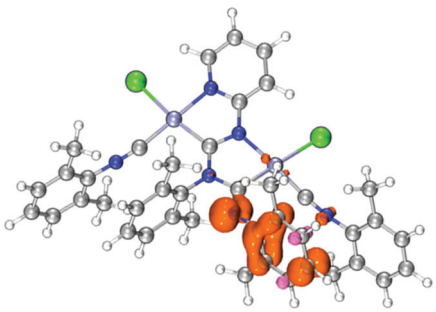

Fig. 5 A plot of the spin density calculated for $[\mathbf{8}]^+$.

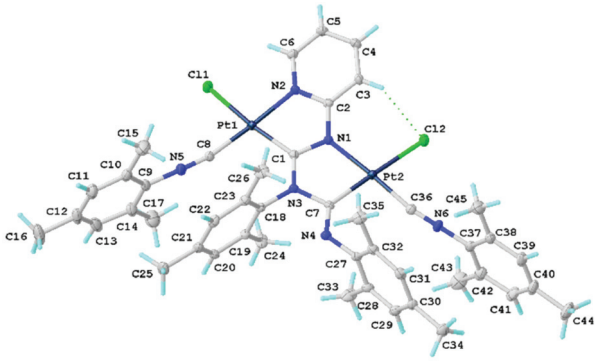

Fig. 6 View of **11** with the atomic numbering schemes. Solvent molecule and hydrogen labels are omitted for simplicity. The crystal data, and selected bond lengths and angles are given in the ESI, section S1.†

symmetry *P*1 space group (Fig. 6). In **11**, both metal centres acquire the distorted square-planar coordination environment. The CNR ligands are at the *cis*-position to the C atoms of {C(NR)N(R)CN(NC$_4$H$_3$X)} (X = CH, N); the latter forms a dinuclear bicyclic framework.

The bond lengths of the two coordinated CN groups are in the interval of 1.136(8)–1.145(8) Å, typical of the CN triple bonds in isocyanide Pd^{II} and Pt^{II} complexes.[3e,24] The Pt–$C_{carbene}$ distances 1.983(6)–1.989(5) Å are slightly smaller than those of typical Pt–C bonds (1.995–2.023 Å)[5d,25] reported for the relevant Pt^{II}–ADC complexes and are close to the Pt–C distances in Pt–NHC complexes (1.970–1.991 Å).[26] On the other hand, the Pt–C bond lengths are sufficiently larger than those in Pt–NHCs, where the NHC is included in the extended rigid π-system (1.906–1.970 Å)[27] and in Pt–CAAC complexes (1.942–1.967 Å).[28] The bond lengths in the first carbene moiety C^1–N^1 (1.349(8) Å) and C^1–N^3 (1.341(7) Å) are similar and are between a single CN bond (*e.g.*, 1.469(10) Å) in amines[29] and a double CN bond (*e.g.*, 1.279(8) Å) in imines,[29] and the distances indicate a substantial delocalization of the electron density. In the second carbene, the endocyclic C^7–N^3 bond of the metallacycle is typically single (1.449(8) Å), while the exocyclic C^7–N^4 bond is typically double (1.264(8) Å) indicating a low degree of delocalisation in this NCN carbene fragment. The structure of this carbene moiety is, therefore, closer to the amino(imino)carbene or diaminocarbene-like structures reported previously.[11,30] All other bond lengths in **11** are normal, and their values agree with those for the previously reported **7**,[10b] **8**[9] and other related diaminocarbene and isocyanide species.[8c,10a,31]

DFT analysis of ligand properties in chloride species 7–12

To shed light on the nature of the bonding in these compounds, the quantum theory of atoms in molecules (QTAIM)[32] and Mayer bond order analysis,[33] as well as the extended transition state and the natural orbitals for chemical valence (ETS-NOCV) method,[34] were used.

Bader's theory of atoms in molecules provides a unique way to analyse the electron density, ρ_u.[32] The most important prop-

erty to assign a bond is the presence of a bond critical point (BCP) which is a point of electron and energy densities along the bond path. It is quite interesting to compare the M^1–C^1 bonds, which involve the metalla-N-heterocyclic carbene C^1 atoms, with the almost equivalent M^2–C^7 bonds, which engage the only formal acyclic diaminocarbene C^7 atom. The BCPs for both pairs of M–$C_{carbene}$ bonds show a moderate value of electron density (ρ_b 0.070–0.091e) and a positive value of the Laplacian (Table S9†). Since a covalent bond in transition metal complexes is characterized by a small value of ρ_b and small and positive values of $\nabla^2\rho(r)$ due to the diffuse character of the electron distribution,[35] the best descriptor to ascertain the type of interaction is the local energy electron density $H(r)$.[36] All of these M–$C_{carbene}$ have negative values of $H(r)$ at the BCPs. The listed parameters indicate a significant degree of covalency. Another similar criterion was proposed by Espinosa[37] on the basis of the ratio $|V(r)|/G(r)$ for closed-shell interactions, $|V(r)|/G(r) < 1$ and for shared shell interactions, $|V(r)|/G(r) > 2$. The interaction is taken as an intermediate type if the ratio falls between these two limits.[38] The BCPs of M–$C_{carbene}$ bonds have $|V(r)|/G(r)$ values of 1.47–1.70 and it is taken as evidence for a partially covalent nature. At the same time, the values for the ρ_b bond and $|V(r)|/G(r)$ for all M–$C_{carbene}$ bonds are higher than those for the M–Cl, M–C_{CNR} and M–N bonds; all this indicates that M–$C_{carbene}$ is more covalent. The values for the local topological properties at the BCP of these two types of M–$C_{carbene}$ bonds are close enough (Table S9†), and are comparable to those obtained from the theoretical electronic energy density for the M–$C_{carbene}$ bonds of the other diaminocarbene complexes.[36,39] The calculated Mayer bond orders (MBOs) of the M–$C_{carbene}$ bonds are similar for both M–$C_{carbene}$ bonds of each complex (0.5491 and 0.5512 for **7** and 0.9907 and 1.0678 for **8**) and are larger than the MBOs of the M–C_{CNR} bonds (0.2675 and 0.2753 for **7** and 0.9029 and 0.9058 for **8**). The values of the topological parameters at BCPs of the $C_{carbene}$–N bonds are all typical of covalent bonds between nonmetal atoms with some degree of delocalization.[40] The MBOs for $C_{carbene}$–N bonds in the N^1–C^1–N^3 moiety are higher than 1 and very similar (1.2570–1.3101), which support the previous proposal that the unsaturation of the C atom of diaminocarbene is alleviated by π-donation of electron density from the filled pπ orbitals of the N atoms to the empty pπ orbital of the carbene carbon.[41] The MBOs for $C_{carbene}$–N bonds in the second N^3–C^7–N^4 moiety are different (0.9715–0.9989 for C^7–N^3 and 1.6346–1.6752 for C^7–N^4) as evidenced by XRD data.

The coordination bonding in binuclear diaminocarbene complexes was rationalised by the extended transition state (ETS)[42] together with the natural orbitals for chemical valence (NOCV)[34,43] method. The ETS-NOCV scheme in this manner gives quantitative (ΔE_{orb}) data on the strength of orbital interactions in chemical bonds.[44] The ETS-NOCV calculations for **7** and **8** were carried out using PBE0/ZORA-def2-TZVP geometries with the ADF program package.[45] The fragmentation pattern is shown in Fig. S13,† where the C^1–N^1, C^7–N^3 and M–L bonds were fragmented homolytically in the frozen geometry of the complex molecule for this purpose. The major contribution to the total orbital interaction comes from the three orbital terms $\Delta E_{orb(1)} - \Delta E_{orb(3)}$ (90%), indicating a strong covalent bonding (Fig. 7). The strongest pairwise orbital interaction ($\Delta E_{orb(1)}$, −470 kcal mol^{-1}) comes from the ligand to metal σ-dative interactions, which is provided by 41% of total ΔE_{Orb}. Then, the second term ($\Delta E_{orb(2)}$, −362 kcal mol^{-1}) is associated with the coupling of p orbitals in diaminocarbene moieties. The last $\Delta E_{orb(3)}$ (−225 kcal mol^{-1}) is due to the π-back-donation from metal centers to carbene ligands and comprises only 20% of the total ΔE_{Orb} energy.

X-Ray diffraction studies of thiocyanate derivatives

Single crystals of **16** and **18** were obtained directly from the reaction mixture upon its slow evaporation (Fig. 8, 9, and S1†).

Compounds **16** and **18** form isomorphs *via* the Pd/Pt atom exchange in the molecular crystals.[5d,24d,e] Both thiocyanates in **16** and **18** are bound to the metals by the N atom in agreement with the IR spectroscopy results. The M^1–N^8 and M^2–N^9 distances were within the range of typical values for Pd–N[16b,46] and Pt–N[16a,46] coordination bonds reported for relevant *N*-ligated thiocyanates. The M^1–N^8–C^{45} and M^2–N^9–C^{46} angles due to the thiocyanate binding are considerably different: one thiocyanate in **16** and **18** is coordinated to the metal in a somewhat linear fashion (M^1–N^8–C^{45} 175.7(3)–178.5(3)°), while the

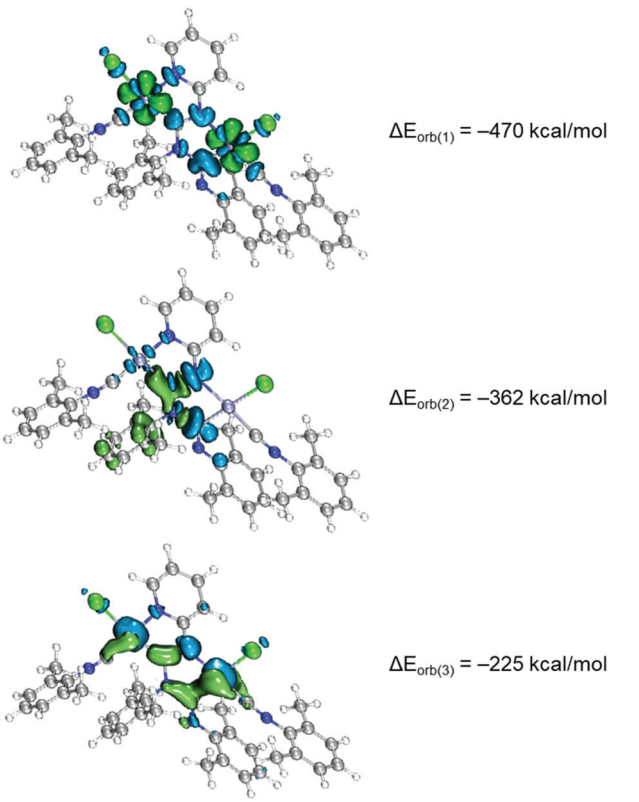

Fig. 7 Shape of the deformation densities $\Delta\rho_{(1)-(3)}$ that correspond to $\Delta E_{orb(1)-(3)}$. The direction of the charge flow of the deformation densities is blue (loss of electron density) → green (gain of electron density).

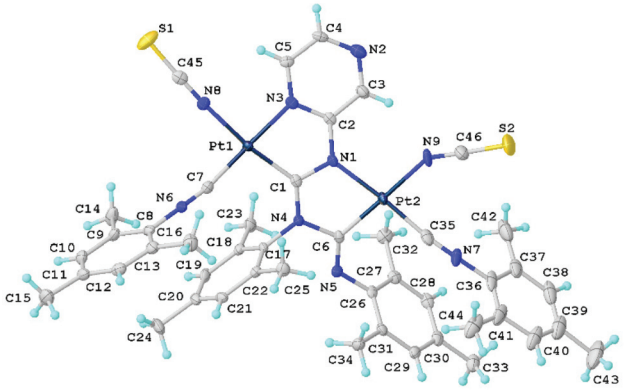

Fig. 8 View of **18** with the atomic numbering schemes. Solvent molecule and hydrogen labels are omitted for simplicity. Crystal structure of **16** is given in section S1 in the ESI† alongside selected bond lengths and angles.

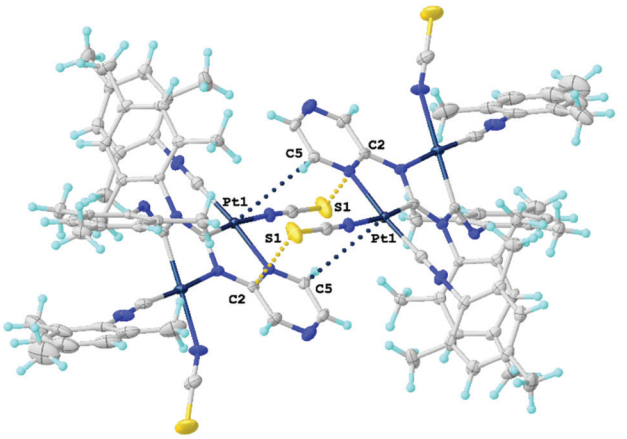

Fig. 9 Views of dimers of **18**. Dotted lines indicate the $Pt^1\cdots C^5$ and $S^1\cdots C^2$ contacts. Thermal ellipsoids are shown with 50% probability.

other adopts a bent configuration (M^2–N^9–C^{46} angle in the range of 147.1(3)–159.1(4)°). Subsequent theoretical studies (section S4.1†) and analysis of the CCDC (section S5†) showed that the differences are associated with the effect of crystal packing.

The polycyclic organometallic skeleton of thiocyanate complexes **16** and **18** is almost identical to that of chloride species (Fig. S2 and S3†). Thiocyanate ligands are explored as potential crystal-driving supramolecular generators in biochemistry[47] and materials[48] studies. The versatile nature of the interacting centers in NCS is mainly associated with sulfur and the nitrogen atoms allow it to be involved in hydrogen bonding,[49] halogen bonding,[50] and π-interactions.[51] The Hirshfeld surface analysis of the XRD structures of **16** and **18** indicates the domination of the contacts that involve hydrogen atoms, specifically, H–H, C–H, S–H, and N–H (section S6 in the ESI†). The H–H contacts provide the largest contributions to the molecular Hirshfeld surfaces, because the fraction of these atoms is maximal and the Hirshfeld surface analysis does not disclose the attractive or repulsive nature of these contacts. Apart from the contacts involving H atoms, **16** and **18** exhibit two pairs $M^1\cdots C^5$ and $S^1\cdots C^2$ short intermolecular contacts forming supramolecular dimers (Fig. 9). The distances between the $M^1\cdots C^5$ and $S^1\cdots C^2$ interacting atoms are slightly larger than the sum of Bondi's vdW radii (102–109%),[52] but are comparable with the sum of Alvarez's (86–89% for $M^1\cdots C^5$ and 98–99% for $S^1\cdots C^2$)[53] vdW radii, confirming the presence of noncovalent interactions. To further confirm the existence of noncovalent interactions between the M^{II}-center and C^5 atom and between the S-center of thiocyanato and C^2 atom, a further computational study was carried out.

QTAIM analysis[32] of model supramolecular associates $(\mathbf{16})_2$ and $(\mathbf{18})_2$ shows appropriate bond critical points (3, −1) (BCPs) for the discussed contacts (Fig. 10, 11, S15, S16 and Table S13†). In the case of $(\mathbf{18})_2$, the formally bifurcated μ_2-S$\cdots$[Pt^{II},C] contact (Fig. 11) and in the case of $(\mathbf{16})_2$ a $S^1\cdots Pd^2$ contact (Fig. S16†) are formed. The low magnitudes of electron density (0.005–0.008 a.u.), the positive values of the Laplacian of electron density (0.015–0.021 a.u.), and the positive energy density close to zero (0.001 a.u.) in the BCPs, as well as the balance between the Lagrangian kinetic energy $G(r)$ and potential energy density $V(r)$ at the BCPs (ratio $|G(r)|/V(r) > 1$), reveal that these contacts are purely noncovalent.[37]

The Electron Localization Function[54] (ELF) projections for the $M^1\cdots C^5$ contacts were plotted along with CPs and bond paths (Fig. 10, 11 and S15, S16†). ELF projections show increased ELF areas around Pd^{II} and Pt^{II} atoms near the bond paths connecting the metal centers and azaheterocyclic species that can be interpreted as filled d_{z^2} orbitals. The M$\cdots$C bond paths that connect the metal centers and C^5 atom from the azaheterocyclic species go through these d_{z^2} and π*-orbitals. In the ELF projections plotted for the $S^1\cdots C^2$ contacts, a

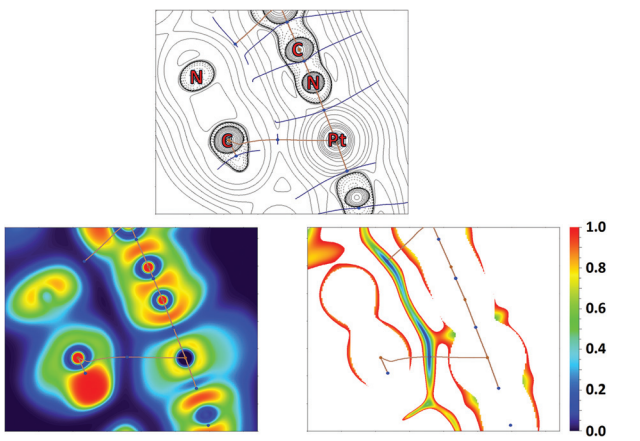

Fig. 10 Contour line diagram of the Laplacian of electron density distribution $\nabla^2\rho(r)$, bond paths, and selected zero-flux surfaces (left panel), visualization of the electron localization function (ELF, center panel) and reduced density gradient (RDG, right panel) analyses of $Pt^1\cdots C^5$ intermolecular contacts in $(\mathbf{18})_2$. Bond critical points (3, −1) are shown in blue, nuclear critical points (3, −3) in pale brown, and bond paths as pale brown lines, length units are Å, and the color scale for the ELF and RDG maps is presented in a.u.

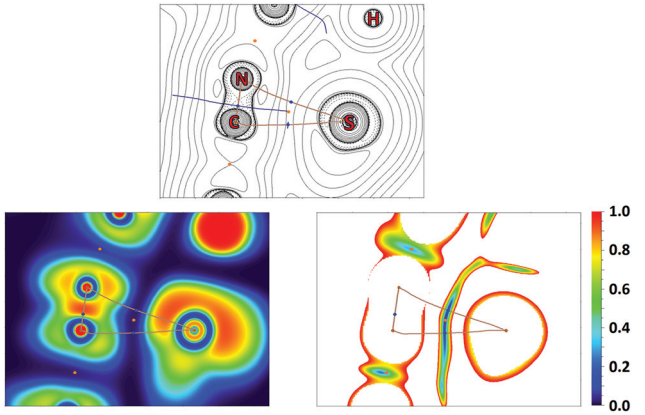

Fig. 11 Contour line diagram of the Laplacian of electron density distribution $\nabla^2\rho(r)$, bond paths, and selected zero-flux surfaces (left panel), visualization of the electron localization function (ELF, center panel) and reduced density gradient (RDG, right panel) analyses of μ_2-S···[Pt^{II},C] intermolecular contacts in $(\mathbf{18})_2$. Bond critical points (3, −1) are shown in blue, nuclear critical points (3, −3) in pale brown, ring critical points (3, +1) in orange, and bond paths as pale brown lines, length units are Å, and the color scale for the ELF and RDG maps is presented in a.u.

sulfur lone pair is visible near the bond paths; also, the electron density depletion regions associated with the π-holes are easily identified in the ELF basins. Reduced density gradient (RDG) analyses confirm the fact that all discussed contacts are attractive.

The comparison of the crystal structures of the thiocyanate derivatives with those of the chloride species (Fig. S4 and S5†) revealed significant changes that occurred on anion exchange. While the crystal structure of the chloride species is predominantly held by C–H···X (X = Cl, N) hydrogen bonds with no involvement of the M^{II}-center, the change from Cl to NCS favours the formation of M···C interactions.

Application of Pt^{II}–MNHC complexes as photocatalysts for hydrosilylation of alkynes

Representative platinum(II) diaminocarbene derivatives **8**, **11** and **12** were evaluated as potential photocatalysts in the hydrosilylation of alkynes. As a model system, we have chosen the reaction of 1,2-diphenylacetylene with triethylsilane giving 1,2-(diphenylvinyl)triethylsilane under the photocatalytic conditions similar to those reported previously.[9]

Without the addition of a catalyst, no reaction was observed in the 20–60 °C range with or without visible light irradiation (Table 1, entries 1–3) indicating that irradiation itself is not sufficient to initiate this process. Furthermore, at 40–60 °C only an insignificant catalytic effect of any studied complexes was observed after 6 h without light (catalyst loading: 0.1 mol%, entries 4–5, 7–8 and 9–12). Under blue LED irradiation all catalysts **8**, **11**, and **12** showed moderate to good activity (62–89% product yields after 6 h, entries 6, 9 and 13); complex **11** was the most active (entry 9; 89% product yield). Increasing the reaction time to 12 h led to nearly quantitative conversion of the starting 1,2-diphenylacetylene to the respective silylated product (entry 14). Application of 0.5 mol% of catalyst shortens the reaction time to 4 h (entry 15), suggesting that the system with higher catalyst loading can be used if shorter reaction time is preferred over a larger TON. Although the exact reasons for the increased catalytic activity of mesityl carbene species require further studies, some first attempts suggest the optimum combination of donor and steric properties of these derivatives.[55]

Table 1 Photocatalytic activities of **8**, **11** and **12** in the model hydrosilylation reaction[a]

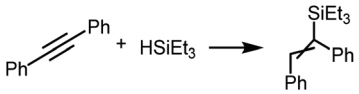

Entry	Catalyst	Product yield[b] At 40 °C, no LED	At 60 °C, no LED	At 40 °C, with LED light
1–3	—	<5	<5	<5
4–6	**8**	<5	5	62
7–9	**11**	<5	6	89
10–13	**12**	<5	<5	81
14	**11**			98[c]
15	**11**			98[d]

[a] Reaction conditions: 1,2-diphenylacetylene (5.0×10^{-4} mol), Et_3SiH (7.5×10^{-4} mol), selected catalyst (5.0×10^{-7} mol, 0.1 mol%), toluene (2 mL), and time: 6 h; for entries with light irradiation a 3 × 2 W LED source with a 445 nm maximum was used. [b] Yield of 1,2-(diphenylvinyl)triethylsilane was determined by ^{1}H NMR spectroscopy using 1,2-dimethoxyethane as the internal standard; the product was obtained as a mixture of *E*/*Z* isomers (*E* 55–75%). [c] Time: 12 h. [d] Catalyst loading: 0.5 mol%, 4 h.

Conclusions

In the course of this study, a series of new binuclear palladium(II) and platinum(II) metalla-N-heterocyclic carbene (MNHC) type complexes were prepared *via* metal-mediated coupling between *cis*-[MCl$_2$(CNR)$_2$] (R = Xyl, Mes) and 2-aminopyridine or 2-aminopyrazine nucleophiles. Structural characterization of **7–12** thus achieved by HRESI$^+$-MS, IR, and 1D (^{1}H, ^{13}C{^{1}H}, ^{195}Pt{^{1}H}) and 2D (^{1}H,^{13}C-HSQC, ^{1}H,^{13}C-HMBC) NMR spectroscopy as well as by single-crystal XRD revealed the difference in diaminocarbene ligands where both C$_{carbene}$–N bonds in the MNHC moiety are in agreement with the data for classical diaminocarbenes, while the second NCN fragment is an ADC-like carbene due to the rather double and single C–N bond character. QTAIM reveals that the M–C$_{carbene}$ bonds are characterized by low to moderate values of electron density ρ_b, positive values of the Laplacian $\nabla^2\rho$, and negative values of local electron energy densities, $H(r)$, signifying that these M–C$_{carbene}$ bonds have a significant degree of covalency. In the UV-vis absorption spectrum of the MNHC species, the wide intense absorption in the 320–414 nm range is assigned to ^{1}L′LCT/^{1}ILCT transitions which are important for visible-light photocatalysis. The absorption characteristics are governed by

the nature of the azaheterocyclic fragment and complexes with pyrazine and pyridine rings (**10** and **12**) show 20–40 nm red-shifted bands relative to their pyrazine counterparts (**7**–**9** and **11**). In contrast, the parent CNR fragments have more effect on the electrochemical properties of the MNHC compounds, and species with mesityl substituents (**9**–**12**) are oxidized at a lower potential than their corresponding xylyl analogues (**7** and **8**).

Moreover, the first palladium(II) and platinum(II) diaminocarbene thiocyanate derivatives **13**–**18** were synthesized from the corresponding starting chlorides **7**–**12** by metathetic reaction with NH_4NCS. In these complexes, both thiocyanate ligands are *N*-bound as confirmed by IR spectroscopy and single-crystal XRD. Replacing both chloride ligands with thiocyanate ligands leads to minor changes in absorption spectra, however, significantly reducing the solubility of compounds in organic solvents. Isomorphous crystal structures of the thiocyanate derivatives **16** and **18** exhibit two symmetrical pairs $M^1\cdots C^5$ and $S^1\cdots C^2$ short intermolecular contacts between the electron-rich M^{II}-center and thiocyanate ligand on the one side, and the electron-poor π system of the azaheterocyclic ring on the other side; the observed noncovalent interactions provide supramolecular dimers.

The photocatalytic properties of the prepared platinum–diaminocarbenes **8**, **11** and **12** as catalysts for hydrosilylation of alkynes with hydrosilanes were evaluated. The highest catalytic efficiency was achieved with complex **11** that is derived from the platinum-mediated coupling of mesityl isocyanide with 2-aminopyridine. The catalytic system uses blue LED irradiation for 6–12 h in toluene with a typical catalyst loading of 0.1 mol% and allows the transformation of 1,2-diphenylacetylene and triethylsilane into the respective 1,2-(diphenylvinyl) triethylsilane with up to 98% yields.

Together, the experimental and computational data provide an insight into the flexible character of the MNHC species. We explored the photocatalytic properties of the [M]–MNHCs derived from reactions of metal-activated RNCs and various 2-aminoazaheterocycles in order to develop useful catalytic systems and to establish catalyst structure–activity relationships for other visible light activated systems,[56] including Pd-catalyzed cross-coupling reactions and Pt-catalyzed hydroarylation reactions.

Experimental

Materials and instrumentation

Solvents, organic and inorganic reagents were obtained from commercial sources and used as received. Isocyanide complexes *cis*-$[MCl_2(CNR)_2]$ (M = Pd, R = Xyl **1**,[11] Mes **2**;[81] M = Pt, R = Xyl **3**,[57] Mes **4**[58]) were prepared as reported earlier. C, H, and N elemental analyses were carried out on a Euro EA 3028 HT CHNSO analyzer. Mass-spectra were acquired on a Bruker micrOTOF spectrometer equipped with an ESI source; a CH_2Cl_2/MeOH mixture was used as the solvent. The instrument was operated in positive ion mode using an *m*/*z* range of 50–3000. The capillary voltage of the ion source was set at −4500 V (ESI^+) and the capillary exit at +(70–150) V. The nebulizer gas pressure was 0.4 bar and drying gas flow was 4.0 L min^{-1}. The most intense peak in the isotopic pattern is reported. Infrared spectra were recorded on a Bruker Tensor 27 FTIR instrument (4000–2400 cm^{-1}, resolution 2 cm^{-1}) using KBr pellets. The UV/vis absorption spectra in CH_2Cl_2 solution were recorded on a Shimadzu UV-2500 spectrophotometer in a quartz cuvette with l = 1.0 mm and the complex's concentration was 0.03 mM. A Shimadzu UV-1800 spectrophotometer was used to measure the UV/vis absorbance of solid-state complexes. The ^{13}C CP/MAS NMR spectra were acquired using a double-resonance 4 mm MAS Bruker probe at a resonance frequency of 101 MHz under 14 kHz MAS. The CP contact time in all experiments was 3.5 μs with a delay between acquisitions of 1 s and the number of scans collected was 20 000. Suitable single crystals were selected and mounted on a MiTeGen tip *via* a crystallographic oil. Data were collected using a Rigaku XtaLAB Synergy, single source at home/near, HyPix diffractometer (monochromated CuKα radiation, λ = 1.54184 Å) at 100 (0) K. In each case, the structure was solved with a ShelXT[59] structure solution program using Intrinsic Phasing and refined with a ShelXL[59] refinement package incorporated in the OLEX^2 program package[60] using Least Squares minimization. Empirical absorption correction was applied in the CrysAlisPro[61] program complex using spherical harmonics, implemented in the SCALE3 ABSPACK scaling algorithm. The CVs were measured using an Autolab PGSTAT302N voltammetric analyzer at a scan rate of 100 mV s^{-1}. Glassy carbon and a platinum wire were used as the working and counter electrodes, respectively. The sample solutions (*ca.* 5 mM) were in 0.1 M $[nBu_4N](BF_4)$–CH_2Cl_2. $Ag/AgNO_3$ (0.01 M $AgNO_3$ in MeCN) was used as the reference electrode and the potential values were corrected against an Fc^+/Fc couple ($E_{1/2}$ = 0.52 V *vs.* $Ag/AgNO_3$ in CH_2Cl_2).

Synthetic work

General procedure for the synthesis of 7–12. A mixture of solid $[MCl_2(CNR)_2]$ (**1**–**4**, 0.10 mmol) and aminoazaheterocycles **5** and **6** (0.20 mmol) was dissolved in CH_2Cl_2 (5 mL) and left to stand at RT for 24 h. During the reaction time, the mixture turned from pale yellow to lemon yellow. After 24 h, the reaction mixture was filtered to remove precipitated **5**·HCl or **6**·HCl and then slowly evaporated in air at RT to give yellow crystals of **7**–**12**. The solids of **7**–**12** were separated by decantation and washed with three 2 mL portions of Et_2O and then dried in air at RT.

9. Yellowish solid (37 mg, yield 78%). Anal. Calcd for $C_{45}H_{48}N_6Cl_2Pd_2$: C, 56.5; H, 5.1; N, 8.8; found: C, 56.7; H, 5.4; N, 9.0. $[M - Cl]^+$ calcd for $C_{45}H_{48}N_6ClPd_2^+$ 921.1703, found 921.1706. IR (KBr, selected bands, cm^{-1}): ν(C–H) 2920 (s), 2854 (s); ν(C≡N) 2189 (s); $\nu(C_{carbene}–N)$ 1629 (s); δ(C–H from Mes) 855 (s). ^1H NMR ($CDCl_3$, 400.13 MHz, δ): 9.10 (d, $^3J_{H,H}$ = 8.5 Hz, 1H, H^3), 9.06–8.99 (m, 1H, H^5), 7.84 (ddd, $^3J_{H,H}$ = 8.8 Hz, $^3J_{H,H}$ = 7.4, $^4J_{H,H}$ = 1.7 Hz, 1H, H^4), 7.03–6.94 (m, 1H, H^6), 6.91 (s, 2H, *m*-H from Mes), 6.82 (s, 2H, *m*-H from Mes), 6.68 (s, 2H, *m*-H from Mes), 6.46 (s, 2H, *m*-H from Mes), 2.41 (s, 6H, 2Me),

2.31 (s, 3H, Me), 2.26 (s, 15H, 3Me), 2.23 (s, 6H, 2Me), 2.02 (s, 6H, 2Me), 1.47 (s, 3H, Me), 1.46 (s, 3H, Me). $^{13}C\{^1H\}$ NMR (101 MHz, $CDCl_3$, δ): 195.0 ($C_{carbene}$–N), 167.0 ($C_{carbene}$–N), 162.8 (C═N), 147.7 (*p*-C from Mes), 146.7, 141.5 (C^3, C^4), 140.7 (*ipso*-C from Mes), 140.0, 139.8, 138.9 (*p*-C from Mes), 136.2, 133.9, 133.9 (*o*-C from Mes), 133.7 (*p*-C from Mes), 128.5, 128.3, 128.1, 127.2 (*m*-C from Mes), 124.9, 124.2 (*ipso*-C from Mes), 118.3, 117.2 (C^5, C^6), 21.2, 21.1, 20.1, 20.0 (Me's), 19.5, 19.3 (2Me's), 18.4 (4Me).

10. Yellow solid (42 mg, yield 88%). Anal. Calcd for $C_{44}H_{47}N_7Cl_2Pd_2$: C, 55.2; H, 5.0; N, 10.2; found: C, 54.8; H, 5.0; N, 10.6. $[M + H]^+$ calcd for $C_{44}H_{48}N_7Cl_2Pd_2^+$ 958.1417, found 958.1412. IR (KBr, selected bands, cm^{-1}): ν(C–H) 2916 (s), 2853 (s); ν(C≡N) 2199 (s), 2189 (s); ν($C_{carbene}$–N) 1632 (s); δ(C–H from Mes) 854 (s). ^1H NMR ($CDCl_3$, 400.13 MHz, δ): 10.37 (d, $^4J_{H,H}$ = 0.7 Hz, 1H, H^3), 8.89 (dd, $^3J_{H,H}$ = 3.1 Hz, $^4J_{H,H}$ = 1.0 Hz, 1H, H^5), 8.32 (d, $^3J_{H,H}$ = 3.3 Hz, 1H, H^6), 6.93 (s, 2H, *m*-H from Mes), 6.83 (s, 2H, *m*-H from Mes), 6.69 (s, 2H, *m*-H from Mes), 6.48 (s, 2H, *m*-H from Mes), 2.40 (s, 6H, 2Me), 2.32 (s, 3H, Me), 2.26 (s, 3H, Me), 2.02 (c, 6H, 2Me), 2.26 (c, 3H, Me), 2.02 (s, 6H, 2Me), 1.47 (s, 6H, 2Me). $^{13}C\{^1H\}$ NMR (101 MHz, $CDCl_3$, δ): 196.8 ($C_{carbene}$–N), 163.2 (*ipso*-C from Mes), 161.8 ($C_{carbene}$–N), 147.6 (*p*-C from Mes), 142.2 (C^3), 140.6 (*p*-C from Mes), 140.2 (*p*-C from Mes), 139.1 (*ipso*-C from Mes), 137.9 (C^5), 137.6 (C^6), 135.9 (*o*-C from Mes), 134.0 (*o*-C from Mes), 133.9 (*ipso*-C from Mes), 133.9 (*o*-C from Mes), 128.6, 128.3, 128.2 (*m*-C from Mes), 127.0 (*o*-C from Mes), 124.7 and 123.9 (C≡N), 21.2, 21.1, 20.1, 20.0, 19.5 (Me's), 19.2 (2Me's), 18.4 (4Me's).

11. Yellow solid (47 mg, yield 83%). Anal. Calcd for $C_{45}H_{48}N_6Cl_2Pt_2$: C, 47.7; H, 4.3; N, 7.4; found: C, 47.2; H, 4.3; N, 7.6. $[M + H]^+$ calcd for $C_{45}H_{49}Cl_2N_6Pt_2^+$ 1134.2688, found 1134.2678. IR (KBr, selected bands, cm^{-1}): ν(C–H) 2915 (s); ν(C≡N) 2194 (s); ν($C_{carbene}$–N) 1667 (s), 1619 (s); δ(C–H from Mes) 771 (s). ^1H NMR ($CDCl_3$, 400.13 MHz, δ): 9.36–9.07 (m, 2H, H^5 + H^3), 8.02–7.73 (m, 1H, H^4), 7.05 (t, $^3J_{H,H}$ = 6.6 Hz, 1H, H^6), 6.92 (s, 2H, *m*-H from Mes), 6.82 (s, 2H, *m*-H from Mes), 6.68 (s, 2H, *m*-H from Mes), 6.42 (s, 2H, *m*-H from Mes), 2.40 (s, 6H, 2Me), 2.32 (s, 3H, Me), 2.27 (s, 15H, 3Me), 2.25 (s, 6H, 2Me), 2.04 (s, 6H, 2Me), 1.45 (s, 3H, Me), 1.40 (s, 3H, Me). $^{13}C\{^1H\}$ NMR (101 MHz, $CDCl_3$, δ): 183.6 ($C_{carbene}$–N), 168.3 ($C_{carbene}$–N), 153.0 (C═N), 148.3 (*p*-C from Mes), 145.1, 141.7 (C^3, C^4), 140.1, (*ipso*-C from Mes), 139.9, 139.6, 138.6 (*p*-C from Mes), 136.2, 134.0, 133.9 (*o*-C from Mes), 133.1 (*p*-C from Mes), 128.5, 128.2, 128.1, 126.7 (*m*-C from Mes), 125.2, 124.6 (*ipso*-C from Mes), 117.7, 116.9 (C^5, C^6), 21.2, 21.1, 20.1, 19.9 (Me's), 19.5, 19.0 (2Me's), 18.4 (4Me's). $^{195}Pt\{^1H\}$ NMR ($CDCl_3$, 86.02 MHz, δ): −3756, −3796.

12. Yellow solid (53 mg, yield 94%). Anal. Calcd for $C_{44}H_{47}N_7Cl_2Pt_2$: C, 46.6; H, 4.2; N, 8.6; found: C, 45.8; H, 4.4; N, 8.4. $[M + H]^+$ calcd for $C_{44}H_{48}N_7Cl_2Pt_2^+$ 1135.2640, found 1135.2644. IR (KBr, selected bands, cm^{-1}): ν(C–H) 2915 (s); ν(C≡N) 2208 (s), 2190 (s); ν($C_{carbene}$–N) 1634 (s); δ(C–H from aryls) 835 (s). ^1H NMR ($CDCl_3$, 400.13 MHz, δ): 10.50 (s, 1H, H^3), 9.10 (d, $^3J_{H,H}$ = 3.0 Hz, 1H, H^6), 8.38 (d, $^3J_{H,H}$ = 3.4 Hz, 1H, H^5), 6.94 (s, 2H, *m*-H from Mes), 6.83 (s, 2H, *m*-H from Mes), 6.70 (s, 2H, *m*-H from Mes), 6.44 (s, 2H, *m*-H from Mes), 2.39 (s, 6H, 2Me), 2.33 (s, 3H, Me), 2.28 (s, 3H, Me), 2.27 (s, 6H, 2Me), 2.25 (s, 6H, 2Me), 2.04 (s, 6H, 2Me), 1.47 (s, 3H, Me), 1.41 (s, 3H, Me). $^{13}C\{^1H\}$ NMR (101 MHz, $CDCl_3$, δ): 185.05 ($C_{carbene}$–N), 162.89 (*ipso*-C from Mes), 153.62 (C^2), 148.11 (*p*-C from Mes), 141.98 (C^3), 141.80 (*p*-C from Mes), 140.20 (*p*-C from Mes), 139.93 (*ipso*-C from Mes), 139.88 (C^3), 138.73 (*p*-C from Mes), 137.06 (C^5), 135.97 (*o*-C from Mes), 135.84 (*o*-C from Mes), 134.34 (C^6), 134.00 (*o*-C from Mes), 133.30 (*ipso*-C from Mes), 132.64 (*ipso*-C from Mes), 129.08 (*o*-C from Mes), 128.58, 128.57, 128.26, 128.09 (*m*-C from Mes), 126.55 (*o*-C from Mes), 125.05 and 124.30 (C≡N), 21.19 (Me's), 21.07 (Me's), 20.06 (Me's), 19.90 (Me's), 19.42 (2Me's), 18.97 (2Me's), 18.32 (4Me's). $^{195}Pt\{^1H\}$ NMR ($CDCl_3$, 86.02 MHz, δ): −3718, −3803.

General procedure for the synthesis of 13–18. A mixture of **7–12** (0.05 mmol) with a three-fold excess of NH_4CNS (0.15 mmol) was suspended in an acetone/CH_2Cl_2 mixture (v/v 3 : 1, 2 mL) at RT. The reaction mixture was stirred overnight to give a yellow solution over the yellow or orange precipitate. These precipitates of **13–18** were separated by centrifugation, washed with two 2 mL portions of H_2O and dried in air at RT.

13. Yellow solid (35 mg, yield 74%). Anal. Calcd for $C_{43}H_{40}N_8S_2Pd_2$: C, 54.6; H, 4.3; N, 11.9; S, 6.8, found C, 54.3; H, 4.8; N, 11.5; S, 6.6. $[M + Na]^+$ calcd for $C_{43}H_{40}N_8S_2Pd_2Na^+$ 969.0784, found 969.0792. IR (KBr, selected bands, cm^{-1}): ν(C≡N) 2204 (s), ν($NC_{thiocyanate}$) 2064, 2087 (s); ν($C_{carbene}$–N) 1605, 1634 (s); δ(C–H from aryls) 778 (s). ^{13}C CP MAS NMR: 136.75, 136.42, 134.39, 133.46, 132.51, 131.36, 130.76, 129.55, 128.80, 127.96, 127.16, 125.82 (C and CH from aryls), 118.49 and 117.77 (C≡N), 21.42, 20.78, 19.03, 18.30 (Me's).

14. Yellow solid (42 mg, yield 75%). Anal. Calcd for $C_{43}H_{40}N_8S_2Pt_2$: C, 46.0; H, 3.6; N, 10.0; S, 5.7, found C, 45.7; H, 3.3; N, 9.8; S, 5.6. $[M - NCS]^+$ calcd for $C_{42}H_{40}N_7SPt_2^+$ 1063.2363, found 1064.2355. IR (KBr, selected bands, cm^{-1}): ν(C≡N) 2202 (s), ν($NC_{thiocyanate}$) 2072, 2094 (s); ν($C_{carbene}$–N) 1611, 1627 (s); δ(C–H from aryls) 777 (s). ^{13}C CP MAS NMR: 166.7, 151.0, 145.1, 144.5, 136.7, 133.7, 130.7, 128.7, 127.9, 126.8, 126.2 (C and CH from aryls), 118.4 and 117.0 (C≡N), 21.5, 20.9, 20.5, 19.0, 18.6, 18.4, 17.8 (Me's).

15. Yellow solid (34 mg, yield 68%). Anal. Calcd for $C_{47}H_{48}N_8S_2Pd_2$: C, 56.3; H, 4.8; N, 11.2; S, 6.4, found C, 55.8; H, 4.3; N, 10.8; S, 6.6. $[M - NCS]^+$ calcd for $C_{46}H_{48}N_7SPd_2^+$ 944.1766, found 944.1754. IR (KBr, selected bands, cm^{-1}): ν(C≡N) 2187 (s), ν($NC_{thiocyanate}$) 2071, 2100 (s); ν($C_{carbene}$–N) 1619 (s); δ(C–H from aryls) 763 (s). ^{13}C CP MAS NMR: 166.2, 140.3, 136.1, 134.8, 129.3, 127.0 (C and CH from aryls), 118.5 and 115.6 (C≡N), 20.0, 19.0 (Me's).

16. Yellow solid (36 mg, yield 71%). Anal. Calcd for $C_{46}H_{47}N_9S_2Pd_2$: C, 55.1; H, 4.7; N, 12.6; S, 6.4, found C, 54.8; H, 4.6; N, 12.8; S, 6.4. $[M - NCS]^+$ calcd for $C_{46}H_{48}N_7SPd_2^+$ 945.1718, found 945.1716. IR (KBr, selected bands, cm^{-1}): ν(C≡N) 2193 (s); ν($NC_{thiocyanate}$) 2057; ν($C_{carbene}$–N) 1625 (s); δ(C–H from aryls) 855 (s). ^{13}C CP MAS NMR: 140.1, 137.9, 135.5, 135.1, 134.2, 133.7, 132.7, 131.5, 128.8 (C and CH from aryls), 19.8, 19.3, 19.1 (Me's).

17. Yellow solid (54 mg, yield 77%). Anal. Calcd for $C_{47}H_{48}N_8S_2Pt_2$: C, 48.0; H, 4.0; N, 9.5; S, 5.4, found C, 47.6; H, 3.7; N, 9.5; S, 5.6. $[M + H]^+$ calcd for $C_{47}H_{49}N_8S_2Pt_2^+$ 1180.2814, found 1180.2820. IR (KBr, selected bands, cm^{-1}): ν(C≡N) 2205 (s), $\nu(NC_{thiocyanate})$ 2030, 2062 (s); $\nu(C_{carbene}–N)$ 1608 (s); δ(C–H from aryls) 854 (s). ^{13}C CP MAS NMR: 196.81 and 190.60 ($C_{carbene}$–N), 160.66, 154.03, 150.48, 141.46, 138.79, 135.41, 133.29, 130.58, 129.43, 127.34, 126.07, 124.60 (C and CH from aryls), 116.12 and 114.59 (C≡N), 20.81, 20.04, 18.11, 16.06 (Me's).

18. Yellow solid (47 mg, yield 80%). Anal. Calcd for $C_{46}H_{48}N_9S_2Pt_2$: C, 46.8; H, 4.0; N, 10.7; S, 5.4, found C, 46.3; H, 3.6; N, 10.6; S, 5.5. $[M + H]^+$ calcd for $C_{46}H_{48}N_9S_2Pt_2^+$ 1180.2750, found 1180.2754. IR (KBr, selected bands, cm^{-1}): ν(C≡N) 2202 (s), $\nu(NC_{thiocyanate})$ 2055, 2097 (s); $\nu(C_{carbene}–N)$ 1604, 1629 (s); δ(C–H from aryls) 845, 860 (s). ^{13}C CP MAS NMR: 185.6 ($C_{carbene}$–N), 161.9, 153.5, 147.5, 145.3, 142.2, 140.8, 140.2, 139.7, 138.0, 136.2, 135.7, 135.1, 134.9, 133.8, 131.2, 130.1, 128.9, 128.4, 128.0, 125.5, 122.7 (C and CH from aryls), 119.0 and 118.4 (C≡N), 24.1, 21.9, 21.4, 19.7, 19.1, 18.4, 17.1 (Me's).

Computational details

DFT/TD-DFT studies on complexes 7, 8, 11 and 12. The full geometry optimization of all complexes was carried out at the DFT level of theory using the PBE0[62] functional with the atom-pairwise dispersion correction with the Becke–Johnson damping scheme (D3BJ)[63] with the help of the ORCA package (version 5.0.2).[64] Zero-order regular approximation (ZORA)[65] was employed to account for relativistic effects. The ZORA-def2-TZVP(-f)[65] basis sets were used for the H, C, N, F, O and S atoms while the SARC-ZORA-TZVP basis sets were used for the Pd and Pt atoms.[66] The Hessian matrix was calculated analytically for the optimized structures to prove the location of correct minima (no imaginary frequencies). A combination of the "resolution of identity" and the "chain of spheres exchange" algorithms (RIJCOSX)[67] in conjunction with the auxiliary basis sets SARC/J was used.[68] The SCF calculations were tightly converged (TightSCF). Numerical integrations during all DFT calculations were performed on a dense grid (DEFGRID3). TD-DFT calculations were performed for optimized geometries in the gas phase and in solution (CH_2Cl_2) using the conductor polarizable continuum model (CPCM)[69] solvation model. Calculation of 60 vertical transition energies to the lowest singlet excited states with significant oscillator strengths and their characteristics allowed us to simulate a large portion of the absorption spectra and are listed in Tables S6 and S7.† Calculations of the lowest 7 singlet–singlet excitation energies at the optimized geometries are satisfied to gain a better insight into the nature of the long wavelength light absorption of the complexes. QTAIM, MOs and spin density were calculated using the Multiwfn 3.8 software[70] and visualized with the VMD program.[71]

DFT studies on complexes 16 and 18. The single point calculations based on the experimental X-ray geometries of **16** and **18** and the full geometry optimization procedure for isolated model structures have been carried out at the DFT level of theory using the dispersion-corrected hybrid functional ωB97XD[72] with also the help of the Gaussian-09[73] program package. For palladium and platinum atoms the quasi-relativistic pseudopotentials MWB28 and MWB60 and the appropriate contracted basis sets[74] were used, and the 6-31G* basis sets were used for other atoms. The topological analysis of the electron density distribution with the help of the atoms in molecules (QTAIM) method developed by Bader[32] has been performed by using the Multiwfn program (version 3.7).[75] The Cartesian atomic coordinates for all model structures are presented in Table S14, ESI.†

Hirshfeld analysis. The Hirshfeld molecular surfaces were generated by the CrystalExplorer17 program.[76] The normalized contact distances, d_{norm},[77] based on Bondi's van der Waals radii,[52] were mapped into the Hirshfeld surface (Table S15 and Fig. S18, S19†). In the color scale, negative values of d_{norm} are visualized with the red color indicating contacts shorter than the sum of van der Waals radii. The white color denotes intermolecular distances that are close to van der Waals contacts with d_{norm} equal to zero. In turn, contacts longer than the sum of van der Waals radii with positive d_{norm} values are colored with blue.

General procedure for catalytic hydrosilylation of alkynes with hydrosilanes (specific conditions are provided in Table 1). The solution of the selected catalyst in CH_2Cl_2 (0.1 mL, 5.0×10^{-6} M) was placed in 5 mm tubes and the solvent was evaporated to dryness under a stream of dinitrogen. 1,2-Diphenylacetylene (5.0×10^{-4} mol), Et_3SiH (7.5×10^{-4} mol), and toluene (2 mL) were added into the tube. The tube was closed with a septum, kept at 40–60 °C or under LED irradiation with 445 nm LEDs (3 × 2 W; the LEDs were placed at a 2 cm distance from the tube) for 6–12 h. The contents of the tube were poured over silica-gel and extracted with hexane (5 mL). The extracts were evaporated under reduced pressure and the crude product was subsequently dissolved in 0.6 mL of $CDCl_3$ with 1,2-dimethoxyethane (1.0 equiv., used as an NMR internal standard) added, and then analyzed by ^1H and ^{13}C NMR spectroscopy. The isomeric content was determined on the basis of the analysis and matching of ^1H and ^{13}C chemical shifts for products against authentic samples of (*E*)-[78] and (*Z*)-1,2-(diphenylvinyl)triethylsilanes.[79] Quantifications were performed upon integration of the selected peaks of the product against peaks of 1,2-dimethoxyethane.

Author contributions

M.V.K. – conceptualisation, investigation (synthesis, physicochemical study and catalysis), and writing; K.V.L. – conceptualisation and writing; E.A.K. – investigation (electrochemical study and computational study of **7**, **8**, **11** and **12**) and writing; A.S.N. – investigation (computational study of **16** and **18**) and writing; M.A.K.– conceptualisation, investigation (catalysis), writing, and project administration.

Conflicts of interest

There are no conflicts to declare.

Acknowledgements

This work was supported by the Russian Science Foundation (project 21-73-10083). The DFT/TD-DFT calculations for studies on **7**, **8**, **11** and **12** were performed by E.A.K. in the framework of the Russian Science Foundation project 21-73-00056, while the electrochemical studies were performed in the framework of the Russian Foundation for Basic Research project 19-29-08026. Measurements were performed at the Center for Magnetic Resonance, Center for X-ray Diffraction Studies, Center for Chemical Analysis, Thermogravimetric and Calorimetric Research Centre, Centre for Optical and Laser Materials Research, Department of Cryogenic Engineering and Materials Research, and Computing Centre (all belong to St Petersburg University).

References

1 (*a*) M. N. Hopkinson, C. Richter, M. Schedler and F. Glorius, An overview of N-heterocyclic carbenes, *Nature*, 2014, **510**, 485; (*b*) H. V. Huynh, Electronic Properties of N-Heterocyclic Carbenes and Their Experimental Determination, *Chem. Rev.*, 2018, **118**, 9457.

2 (*a*) M. A. Kinzhalov and K. V. Luzyanin, Synthesis and Contemporary Applications of Platinum Group Metals Complexes with Acyclic Diaminocarbene Ligands, *Russ. J. Inorg. Chem.*, 2022, **67**, 48; (*b*) M. A. Kinzhalov and K. V. Luzyanin, Reactivity of acyclic diaminocarbene ligands, *Coord. Chem. Rev.*, 2019, **399**, 213014.

3 (*a*) V. P. Boyarskiy, K. V. Luzyanin and V. Y. Kukushkin, Acyclic diaminocarbenes (ADCs) as a promising alternative to N-heterocyclic carbenes (NHCs) in transition metal catalyzed organic transformations, *Coord. Chem. Rev.*, 2012, **256**, 2029; (*b*) L. M. Slaughter, Acyclic Aminocarbenes in Catalysis, *ACS Catal.*, 2012, **2**, 1802; (*c*) E. Peris, Smart N-Heterocyclic Carbene Ligands in Catalysis, *Chem. Rev.*, 2018, **118**, 9988; (*d*) S. A. Timofeeva, M. A. Kinzhalov, E. A. Valishina, K. V. Luzyanin, V. P. Boyarskiy, T. M. Buslaeva, M. Haukka and V. Y. Kukushkin, Application of palladium complexes bearing acyclic amino (hydrazido)carbene ligands as catalysts for copper-free Sonogashira cross-coupling, *J. Catal.*, 2015, **329**, 449–456; (*e*) M. A. Kinzhalov, K. V. Luzyanin, V. P. Boyarskiy, M. Haukka and V. Y. Kukushkin, ADC-Based Palladium Catalysts for Aqueous Suzuki–Miyaura Cross-Coupling Exhibit Greater Activity than the Most Advantageous Catalytic Systems, *Organometallics*, 2013, **32**, 5212.

4 (*a*) M. A. Kinzhalov, E. V. Grachova and K. V. Luzyanin, Tuning the luminescence of transition metal complexes with acyclic diaminocarbene ligands, *Inorg. Chem. Front.*, 2022, **9**, 417–439; (*b*) M. Elie, J. L. Renaud and S. Gaillard, N-Heterocyclic carbene transition metal complexes in light emitting devices, *Polyhedron*, 2018, **140**, 158; (*c*) R. Visbal and M. C. Gimeno, N-heterocyclic carbene metal complexes: photoluminescence and applications, *Chem. Soc. Rev.*, 2014, **43**, 3551.

5 (*a*) I. Ott, in *Advances in Inorganic Chemistry*, ed. P. J. Sadler and R. van Eldik, Academic Press, 2020, vol. 75, p. 121; (*b*) W. Liu and R. Gust, Update on metal N-heterocyclic carbene complexes as potential anti-tumor metallodrugs, *Coord. Chem. Rev.*, 2016, **329**, 191; (*c*) S. A. Patil, A. P. Hoagland, S. A. Patil and A. Bugarin, N-heterocyclic carbene-metal complexes as bio-organometallic antimicrobial and anticancer drugs, an update (2015–2020), *Future Med. Chem.*, 2020, **12**, 2239; (*d*) T. V. Serebryanskaya, M. A. Kinzhalov, V. Bakulev, G. Alekseev, A. Andreeva, P. V. Gushchin, A. Protas, A. Smirnov, T. L. Panikorovskii, P. Lippmann, I. Ott, C. M. Verbilo, A. Zuraev, A. S. Bunev, V. Boyarskiy and N. A. Kasyanenko, Water Soluble Palladium(II) and Platinum(II) Acyclic Diaminocarbene Complexes: Solution Behavior, DNA Binding, and Antiproliferative Activity, *New J. Chem.*, 2020, **44**, 5762.

6 J. Ruiz, L. García, B. F. Perandones and M. Vivanco, A Fischer Carbene within an Arduengo Carbene, *Angew. Chem., Int. Ed.*, 2011, **50**, 3010.

7 J. Ruiz, L. Garcia, C. Mejuto, M. Vivanco, M. R. Diaz and S. Garcia-Granda, Strong electron-donating metalla-N-heterocyclic carbenes, *Chem. Commun.*, 2014, **50**, 2129.

8 (*a*) A. A. Eremina, M. A. Kinzhalov, E. A. Katlenok, A. S. Smirnov, E. V. Andrusenko, E. A. Pidko, V. V. Suslonov and K. V. Luzyanin, Phosphorescent Iridium(III) Complexes with Acyclic Diaminocarbene Ligands as Chemosensors for Mercury, *Inorg. Chem.*, 2020, **59**, 2209; (*b*) A. S. Mikherdov, A. S. Novikov, M. A. Kinzhalov, V. P. Boyarskiy, G. L. Starova, A. Y. Ivanov and V. Y. Kukushkin, Halides Held by Bifurcated Chalcogen–Hydrogen Bonds. Effect of μ(S,N–H)Cl Contacts on Dimerization of Cl(carbene)Pd^{II} Species, *Inorg. Chem.*, 2018, **57**, 3420; (*c*) A. S. Mikherdov, M. A. Kinzhalov, A. S. Novikov, V. P. Boyarskiy, I. A. Boyarskaya, M. S. Avdontceva and V. Y. Kukushkin, Ligation-Enhanced π-Hole···π Interactions Involving Isocyanides: Effect of π-Hole···π Noncovalent Bonding on Conformational Stabilization of Acyclic Diaminocarbene Ligands, *Inorg. Chem.*, 2018, **57**, 6722; (*d*) A. S. Mikherdov, M. A. Kinzhalov, A. S. Novikov, V. P. Boyarskiy, I. A. Boyarskaya, D. V. Dar'in, G. L. Starova and V. Y. Kukushkin, Difference in Energy between Two Distinct Types of Chalcogen Bonds Drives Regioisomerization of Binuclear (Diaminocarbene)PdII Complexes, *J. Am. Chem. Soc.*, 2016, **138**, 14129; (*e*) M. A. Kinzhalov, A. S. Legkodukh, T. B. Anisimova, A. S. Novikov, V. V. Suslonov, K. V. Luzyanin and V. Y. Kukushkin, Tetrazol-5-ylidene Gold(III) Complexes from Sequential [2 + 3] Cycloaddition of Azide to Metal-Bound Isocyanides and N4 Alkylation, *Organometallics*, 2017, **36**, 3974; (*f*) B. G. M. Rocha, E. A. Valishina,

R. S. Chay, M. F. C. Guedes da Silva, T. M. Buslaeva, A. J. L. Pombeiro, V. Y. Kukushkin and K. V. Luzyanin, ADC-metal complexes as effective catalysts for hydrosilylation of alkynes, *J. Catal.*, 2014, **309**, 79.

9 J. C. Gee, B. A. Fuller, H.-M. Lockett, G. Sedghi, C. M. Robertson and K. V. Luzyanin, Visible light accelerated hydrosilylation of alkynes using platinum–[acyclic diaminocarbene] photocatalysts, *Chem. Commun.*, 2018, **54**, 9450.

10 (*a*) M. A. Kinzhalov, K. V. Luzyanin, V. P. Boyarskiy, M. Haukka and V. Y. Kukushkin, Coupling of C-amino aza-substituted heterocycles with an isocyanide ligand in palladium(II) complex, *Russ. Chem. Bull.*, 2013, **62**, 758; (*b*) A. G. Tskhovrebov, K. V. Luzyanin, F. M. Dolgushin, M. F. C. Guedes da Silva, A. J. L. Pombeiro and V. Y. Kukushkin, Novel Reactivity Mode of Metal Diaminocarbenes: Palladium(II)-Mediated Coupling between Acyclic Diaminocarbenes and Isonitriles Leading to Dinuclear Species, *Organometallics*, 2011, **30**, 3362.

11 K. V. Luzyanin, A. J. L. Pombeiro, M. Haukka and V. Y. Kukushkin, Coupling between 3-Iminoisoindolin-1-ones and Complexed Isonitriles as a Metal-mediated Route to a Novel Type of Palladium and Platinum Iminocarbene Species, *Organometallics*, 2008, **27**, 5379.

12 R. Jothibasu, K.-W. Huang and H. V. Huynh, Synthesis of cis- and trans-Diisothiocyanato−Bis(NHC) Complexes of Nickel(II) and Applications in the Kumada−Corriu Reaction, *Organometallics*, 2010, **29**, 3746.

13 M. V. Baker, P. J. Barnard, S. K. Brayshaw, J. L. Hickey, B. W. Skelton and A. H. White, Synthetic, structural and spectroscopic studies of (pseudo)halo(1,3-di-tert-butylimidazol-2-ylidine)gold complexes, *Dalton Trans.*, 2005, 37–43.

14 (*a*) F. De Angelis, S. Fantacci, A. Selloni and M. K. Nazeeruddin, Time dependent density functional theory study of the absorption spectrum of the [Ru(4,4′-COO−-2,2′-bpy)$_2$(X)$_2$]$^{4-}$ (X=NCS, Cl) dyes in water solution, *Chem. Phys. Lett.*, 2005, **415**, 115; (*b*) M. K. Nazeeruddin, S. M. Zakeeruddin, R. Humphry-Baker, S. I. Gorelsky, A. B. P. Lever and M. Grätzel, Synthesis, spectroscopic and a ZINDO study of cis- and trans-(X$_2$)bis(4,4′-dicarboxylic acid-2,2′-bipyridine)ruthenium(II) complexes (X=Cl$^-$, H_2O, NCS$^-$), *Coord. Chem. Rev.*, 2000, **208**, 213.

15 (*a*) K.-H. Chen, T.-H. Lin, T.-E. Hsu, Y.-J. Li, G.-H. Chen, W.-J. Leu, J.-H. Guh, C.-H. Lin and J.-H. Huang, Ruthenium (II) complexes containing dehydroacetic acid and its imine derivative ligands. Synthesis, characterization and cancer cell growth anti-proliferation activity (GI50) study, *J. Org. Chem.*, 2018, **871**, 150; (*b*) F. Nasouti and A. Eslami, Thermoanalytical Study of Linkage Isomerism in Coordination Compounds. Part 7. A DSC and DFT Investigation of Solid-state Linkage Isomerization in Bis (thiocyanato)-bipyridineplatinum(II) Complex, *Z. Anorg. Allg. Chem.*, 2017, **643**, 1131; (*c*) M. A. Fernandes, G. Z. Mashabane, R. Weber and L. Carlton, Structural study of analogues of Wilkinson's compound [Rh(x)(PPh$_3$)$_3$] (X = NCO, NCS, N_3, N(CN)$_2$) and derivatives [Rh(NCO)(O2)(PPh$_3$)$_3$] and [Rh(η^6-C$_6$H$_5$B(NCO)Ph$_2$)(PPh$_3$)$_2$], *Polyhedron*, 2020, **181**, 114468.

16 (*a*) S. Kishi and M. Kato, Thermal and Photo Control of the Linkage Isomerism of Bis(thiocyanato)(2,2′-bipyridine) platinum(II), *Inorg. Chem.*, 2003, **42**, 8728; (*b*) A. J. Paviglianiti, D. J. Minn, W. C. Fultz and J. L. Burmeister, The conjunctive response to steric hindrance in dithiocyanato[bis(diphenylphosphino)alkyl or aryl]palladium(II) complexes: a new look at a classic series, *Inorg. Chim. Acta*, 1989, **159**, 65; (*c*) K. Nakamoto, *Infrared and Raman Spectra of Inorganic and Coordination Compounds: Part A: Theory and Applications in Inorganic Chemistry*, John Wiley & Sons, Inc., 6th edn, 2008.

17 (*a*) J. Yasuda, K. Inoue, K. Mizuno, S. Arai, K. Uehara, A. Kikuchi, Y.-N. Yan, K. Yamanishi, Y. Kataoka, M. Kato, A. Kawai and T. Kawamoto, Photooxidation Reactions of Cyclometalated Palladium(II) and Platinum(II) Complexes, *Inorg. Chem.*, 2019, **58**, 15720; (*b*) K. Karami, A. Ramezanpour, M. Zakariazadeh and C. Silvestru, Catalytic activity and facile recovery of a cyclometalated N-heterocyclic carbene palladium(II) complex immobilized by non-covalent interactions on reduced graphene oxide, *Appl. Organomet. Chem.*, 2019, **33**, e4907; (*c*) M. Iliş, M. Micutz and V. Cîrcu, Luminescent palladium(II) metallomesogens based on cyclometalated Schiff bases and N-benzoyl thiourea derivatives as co-ligands, *J. Org. Chem.*, 2017, **836–837**, 81; (*d*) K. Peng, D. Moreth and U. Schatzschneider, C^N^N Coordination Accelerates the iClick Reaction of Square-Planar Palladium(II) and Platinum(II) Azido Complexes with Electron-Poor Alkynes and Enables Cycloaddition with Terminal Alkynes, *Organometallics*, 2021, **40**, 2584.

18 (*a*) V. Sivchik, R. K. Sarker, Z.-Y. Liu, K.-Y. Chung, E. V. Grachova, A. J. Karttunen, P.-T. Chou and I. O. Koshevoy, Improvement of the Photophysical Performance of Platinum-Cyclometalated Complexes in Halogen-Bonded Adducts, *Chem. – Eur. J.*, 2018, **24**, 11475; (*b*) A. K.-W. Chan, M. Ng, Y.-C. Wong, M.-Y. Chan, W.-T. Wong and V. W.-W. Yam, Synthesis and Characterization of Luminescent Cyclometalated Platinum (II) Complexes with Tunable Emissive Colors and Studies of Their Application in Organic Memories and Organic Light-Emitting Devices, *J. Am. Chem. Soc.*, 2017, **139**, 10750.

19 D. A. Skoog, S. R. Crouch and F. J. Holler, *Principles of instrumental analysis*, Thomson Brooks/Cole, Belmont, CA, 6th edn., 2007.

20 N. Deibel, S. Hohloch, M. G. Sommer, D. Schweinfurth, F. Ehret, P. Braunstein and B. Sarkar, Electrochromic Platinum(II) Complexes Derived from Azobenzene and Zwitterionic Quinonoid Ligands: Electronic and Geometric Structures, *Organometallics*, 2013, **32**, 7366.

21 (*a*) Y. Zhao and D. G. Truhlar, Benchmark Energetic Data in a Model System for Grubbs II Metathesis Catalysis and Their Use for the Development, Assessment, and Validation of Electronic Structure Methods, *J. Chem. Theory Comp.*, 2009, **5**, 324; (*b*) R. Valero, R. Costa,

I. d. P. R. Moreira, D. G. Truhlar and F. Illas, Performance of the M06 family of exchange-correlation functionals for predicting magnetic coupling in organic and inorganic molecules, *J. Chem. Phys.*, 2008, **128**, 114103; (*c*) R. Srivastava and L. R. Joshi, The effect of substituted 1,2,4-triazole moiety on the emission, phosphorescent properties of the blue emitting heteroleptic iridium(III) complexes and the OLED performance: a theoretical study, *Phys. Chem. Chem. Phys.*, 2014, **16**, 17284; (*d*) C. Adamo and D. Jacquemin, The calculations of excited-state properties with Time-Dependent Density Functional Theory, *Chem. Soc. Rev.*, 2013, **42**, 845.

22 P. S. Wagenknecht and P. C. Ford, Metal centered ligand field excited states: Their roles in the design and performance of transition metal based photochemical molecular devices, *Coord. Chem. Rev.*, 2011, **255**, 591.

23 Y. B. Dudkina, D. Y. Mikhaylov, T. V. Gryaznova, A. I. Tufatullin, O. N. Kataeva, D. A. Vicic and Y. H. Budnikova, Electrochemical Ortho Functionalization of 2-Phenylpyridine with Perfluorocarboxylic Acids Catalyzed by Palladium in Higher Oxidation States, *Organometallics*, 2013, **32**, 4785.

24 (*a*) M. V. Kashina, D. M. Ivanov and M. A. Kinzhalov, The Isocyanide Complexes cis-[MCl2(CNC6H4–4-X)2] (M = Pd, Pt; X = Cl, Br) as Tectons in Crystal Engineering Involving Halogen Bonds, *Crystals*, 2021, **11**, 799; (*b*) M. Bulatova, D. M. Ivanov, J. M. Rautiainen, M. A. Kinzhalov, K.-N. Truong, M. Lahtinen and M. Haukka, Studies of Nature of Uncommon Bifurcated I–I···(I–M) Metal-Involving Noncovalent Interaction in Palladium(II) and Platinum(II) Isocyanide Cocrystals, *Inorg. Chem.*, 2021, **60**, 13200; (*c*) A. V. Buldakov, M. A. Kinzhalov, M. A. Kryukova, D. M. Ivanov, A. S. Novikov, A. S. Smirnov, G. L. Starova, N. A. Bokach and V. Y. Kukushkin, Isomorphous Series of PdII-Containing Halogen Bond Donors Exhibiting Cl/Br/I Triple Halogen Isostructural Exchange, *Cryst. Growth Des.*, 2020, **3**, 1975; (*d*) M. A. Kryukova, D. M. Ivanov, M. A. Kinzhalov, A. S. Novikov, A. S. Smirnov, N. A. Bokach and V. Y. Kukushkin, Four-Center Nodes: Supramolecular Synthons Based on Cyclic Halogen Bonding, *Chem. – Eur. J.*, 2019, **25**, 13671; (*e*) M. V. Kashina, M. A. Kinzhalov, A. S. Smirnov, D. M. Ivanov, A. S. Novikov and V. Y. Kukushkin, Dihalomethanes as Bent Bifunctional XB/XB-Donating Building Blocks for Construction of Metal-involving Halogen Bonded Hexagons, *Chem. - Asian J.*, 2019, **14**, 3915; (*f*) M. A. Kinzhalov, M. V. Kashina, A. S. Mikherdov, E. A. Mozheeva, A. S. Novikov, A. S. Smirnov, D. M. Ivanov, M. A. Kryukova, A. Y. Ivanov, S. N. Smirnov, V. Y. Kukushkin and K. V. Luzyanin, Dramatically Enhanced Solubility of Halide-Containing Organometallic Species in Diiodomethane: The Role of Solvent···Complex Halogen Bonding, *Angew. Chem., Int. Ed.*, 2018, **57**, 12785.

25 (*a*) B. G. M. Rocha, E. A. Valishina, R. S. Chay, M. F. C. Guedes da Silva, T. M. Buslaeva, A. J. L. Pombeiro, V. Y. Kukushkin and K. V. Luzyanin, ADC-metal complexes as effective catalysts for hydrosilylation of alkynes, *J. Catal.*, 2014, **309**, 79; (*b*) R. S. Chay, B. G. M. Rocha, A. J. L. Pombeiro, V. Y. Kukushkin and K. V. Luzyanin, Platinum Complexes with Chelating Acyclic Aminocarbene Ligands Work as Catalysts for Hydrosilylation of Alkynes, *ACS Omega*, 2018, **3**, 863.

26 (*a*) S. Diez-Gonzalez, N. Marion and S. P. Nolan, N-Heterocyclic Carbenes in Late Transition Metal Catalysis, *Chem. Rev.*, 2009, **109**, 3612; (*b*) C. P. Newman, R. J. Deeth, G. J. Clarkson and J. P. Rourke, Synthesis of Mixed NHC/L Platinum(II) Complexes: Restricted Rotation of the NHC Group, *Organometallics*, 2007, **26**, 6225; (*c*) J. W. K. Seah, J. X. T. Lee, Y. Li, S. A. Pullarkat, N. S. Tan and P.-H. Leung, Chelating Phosphine–N-Heterocyclic Carbene Platinum Complexes via Catalytic Asymmetric Hydrophosphination and Their Cytotoxicity Toward MKN74 and MCF7 Cancer Cell Lines, *Inorg. Chem.*, 2021, **60**, 17276.

27 A. Tronnier, U. Heinemeyer, S. Metz, G. Wagenblast, I. Muenster and T. Strassner, Heteroleptic platinum(II) NHC complexes with a C^C* cyclometalated ligand – synthesis, structure and photophysics, *J. Mater. Chem. C*, 2015, **3**, 1680.

28 (*a*) S. Roy, K. C. Mondal, J. Meyer, B. Niepötter, C. Köhler, R. Herbst-Irmer, D. Stalke, B. Dittrich, D. M. Andrada, G. Frenking and H. W. Roesky, Synthesis, Characterization, and Theoretical Investigation of Two-Coordinate Palladium(0) and Platinum(0) Complexes Utilizing π-Accepting Carbenes, *Chem. – Eur. J.*, 2015, **21**, 9312; (*b*) S. Roy, K. C. Mondal and H. W. Roesky, Cyclic Alkyl(amino) Carbene Stabilized Complexes with Low Coordinate Metals of Enduring Nature, *Acc. Chem. Res.*, 2016, **49**, 357.

29 F. H. Allen, O. Kennard, D. G. Watson, L. Brammer, A. G. Orpen and R. Taylor, Tables of bond lengths determined by X-ray and neutron diffraction. Part 1. Bond lengths in organic compounds, *J. Chem. Soc., Perkin Trans. 2*, 1987, S1.

30 R. S. Chay, K. V. Luzyanin, V. Y. Kukushkin, M. F. C. Guedes da Silva and A. J. L. Pombeiro, Novel Palladium–Aminocarbene Species Derived from Metal-Mediated Coupling of Isonitriles and 1,3-Diiminoisoindoline: Synthesis and Catalytic Application in Suzuki–Miyaura Cross-Coupling, *Organometallics*, 2012, **31**, 2379.

31 (*a*) S. A. Katkova, M. A. Kinzhalov, P. M. Tolstoy, A. S. Novikov, V. P. Boyarskiy, A. Y. Ananyan, P. V. Gushchin, M. Haukka, A. A. Zolotarev, A. Y. Ivanov, S. S. Zlotsky and V. Y. Kukushkin, Diversity of Isomerization Patterns and Protolytic Forms in Aminocarbene PdII and PtII Complexes Formed upon Addition of N,N′-Diphenylguanidine to Metal-Activated Isocyanides, *Organometallics*, 2017, **36**, 4145; (*b*) M. A. Kinzhalov, S. A. Timofeeva, K. V. Luzyanin, V. P. Boyarskiy, A. A. Yakimanskiy, M. Haukka and

V. Y. Kukushkin, Palladium(II)-Mediated Addition of Benzenediamines to Isocyanides: Generation of Three Types of Diaminocarbene Ligands Depending on the Isomeric Structure of the Nucleophile, *Organometallics*, 2016, **35**, 218; (*c*) E. A. Valishina, M. F. C. Guedes da Silva, M. A. Kinzhalov, S. A. Timofeeva, T. M. Buslaeva, M. Haukka, A. J. L. Pombeiro, V. P. Boyarskiy, V. Y. Kukushkin and K. V. Luzyanin, Palladium-ADC complexes as efficient catalysts in copper-free and room temperature Sonogashira coupling, *J. Mol. Catal. A: Chem.*, 2014, **395**, 162–171; (*d*) M. A. Kinzhalov, V. P. Boyarskiy, K. V. Luzyanin, F. M. Dolgushin and V. Y. Kukushkin, Metal-mediated coupling of a coordinated isocyanide and indazoles, *Dalton Trans.*, 2013, **42**, 10394.

32 R. F. W. Bader, A quantum theory of molecular structure and its applications, *Chem. Rev.*, 1991, **91**, 893.

33 A. J. Bridgeman, G. Cavigliasso, L. R. Ireland and J. Rothery, The Mayer bond order as a tool in inorganic chemistry, *Dalton Trans.*, 2001, 2095.

34 M. P. Mitoraj, A. Michalak and T. Ziegler, A Combined Charge and Energy Decomposition Scheme for Bond Analysis, *J. Chem. Theory Comput.*, 2009, **5**, 962.

35 L. J. Farrugia, C. Evans and M. Tegel, Chemical Bonds without "Chemical Bonding"? A Combined Experimental and Theoretical Charge Density Study on an Iron Trimethylenemethane Complex, *J. Phys. Chem. A*, 2006, **110**, 7952.

36 A. K. Guha, C. Das and A. K. Phukan, Heterocyclic carbenes of diverse flexibility: A theoretical insight, *J. Org. Chem.*, 2011, **696**, 586.

37 E. Espinosa, I. Alkorta, J. Elguero and E. Molins, From weak to strong interactions: A comprehensive analysis of the topological and energetic properties of the electron density distribution involving X–H···F–Y systems, *J. Chem. Phys.*, 2002, **117**, 5529.

38 A. Shahi and E. Arunan, Hydrogen bonding, halogen bonding and lithium bonding: an atoms in molecules and natural bond orbital perspective towards conservation of total bond order, inter- and intra-molecular bonding, *Phys. Chem. Chem. Phys.*, 2014, **16**, 22935.

39 (*a*) K. R. Geethalakshmi, X. Yang, Q. Sun, T. Y. Ng and D. Wang, The nature of interfacial binding of imidazole and carbene ligands with M20 nanoclusters (M = Au, Ag and Cu) – a theoretical study, *RSC Adv.*, 2015, **5**, 88625; (*b*) G. F. Caramori, L. C. Garcia, D. M. Andrada and G. Frenking, Ruthenium(II) complexes of N-heterocyclic carbenes derived from imidazolium-linked cyclophanes, *Dalton Trans.*, 2014, **43**, 14710.

40 R. F. W. Bader, A Bond Path: A Universal Indicator of Bonded Interactions, *J. Phys. Chem. A*, 1998, **102**, 7314.

41 L. E. Johnson and D. B. DuPré, QTAIM Analysis of Ligand Properties and Mechanisms of Tuning of 6-Membered Ring N-Heterocyclic Carbenes in Transition Metal Complexes through Ring-Substituent Variation, *J. Phys. Chem. A*, 2009, **113**, 8647.

42 T. Ziegler and A. Rauk, On the calculation of bonding energies by the Hartree Fock Slater method, *Theor. Chim. Acta*, 1977, **46**, 1.

43 M. Mitoraj and A. Michalak, Donor–Acceptor Properties of Ligands from the Natural Orbitals for Chemical Valence, *Organometallics*, 2007, **26**, 6576.

44 (*a*) G. Frenking and S. Shaik, *The Chemical Bond: Fundamental Aspects of Chemical Bonding*, Wiley, 2014; (*b*) L. Zhao, M. von Hopffgarten, D. M. Andrada and G. Frenking, Energy decomposition analysis, *Wiley Interdiscip. Rev.: Comput. Mol. Sci.*, 2018, **8**, e1345; (*c*) L. Zhao, S. Pan, N. Holzmann, P. Schwerdtfeger and G. Frenking, Chemical Bonding and Bonding Models of Main-Group Compounds, *Chem. Rev.*, 2019, **119**, 8781.

45 A. Bérces, C. Bo, P. M. Boerrigter, L. Cavallo, D. P. Chong, L. Deng, R. M. Dickson, D. E. Ellis, L. Fan, T. H. Fischer, C. Fonseca Guerra, S. J. A. van Gisbergen, J. A. Groeneveld, O. V. Gritsenko, M. Grüning, F. E. Harris, P. van den Hoek, H. Jacobsen, G. van Kessel, F. Kootstra, E. van Lenthe, D. A. McCormack, V. P. Osinga, S. Patchkovskii, P. H. T. Philipsen, D. Post, C. C. Pye, W. Ravenek, P. Ros, P. R. T. Schipper, G. Schreckenbach, J. G. Snijders, M. Sola, M. Swart, D. Swerhone, G. te Velde, P. Vernooijs, L. Versluis, O. Visser, E. van Wezenbeek, G. Wiesenekker, S. K. Wolff, T. K. Woo, E. J. Baerends, J. Autschbach and T. Ziegler, TADF2017; SCM, Theoretical Chemistry, Vrije Universiteit: Amsterdam, The Netherlands, 2017.

46 X. Chang, K.-E. Lee, S. Il Jeon, Y.-J. Kim, H.-K. Lee and S. W. Lee, Bis(isothiocyanato)bis(phosphine) complexes of group 10 metals: reactivity toward organic isocyanides, *Dalton Trans.*, 2005, 3722.

47 L. Tchertanov, Understanding the Peculiarities of Azide and Thiocyanate Binding in Proteins: Use of the Small Molecule Structural Data, *Supramol. Chem.*, 2000, **12**, 67.

48 (*a*) C. Wechwithayakhlung, D. M. Packwood, J. Chaopaknam, P. Worakajit, S. Ittisanronnachai, N. Chanlek, V. Promarak, K. Kongpatpanich, D. J. Harding and P. Pattanasattayavong, Tin(II) thiocyanate $Sn(NCS)_2$ – a wide band gap coordination polymer semiconductor with a 2D structure, *J. Mater. Chem. C*, 2019, **7**, 3452; (*b*) P. Ghorai, P. Brandão, A. Bauzá, A. Frontera and A. Saha, Anion-reliant structural versatility of novel cadmium(II) complexes: Synthesis, crystal structures, photoluminescence properties and exploration of unusual O···S chalcogen bonding involving thiocyanate coligand, *Inorg. Chim. Acta*, 2018, **469**, 189.

49 L. Tchertanov and C. Pascard, Statistical Analysis of Noncovalent Interactions of Anion Groups in Crystal Structures. III. Metal Complexes of Thiocyanate and their Hydrogen-Donor Accepting Function, *Acta Crystallogr., Sect. B: Struct. Sci.*, 1997, **53**, 904.

50 P. Cauliez, V. Polo, T. Roisnel, R. Llusar and M. Fourmigué, The thiocyanate anion as a polydentate halogen bond acceptor, *CrystEngComm*, 2010, **12**, 558.

51 (*a*) J. Wilson, T. Maxson, I. Wright, M. Zeller and S. V. Rosokha, Diversity and uniformity in anion–π com-

plexes of thiocyanate with aromatic, olefinic and quinoidal π-acceptors, *Dalton Trans.*, 2020, **49**, 8734; (*b*) J. Echeverría, Intermolecular Interactions between Thiocyanato Ligands in Metal Complexes, *Cryst. Growth Des.*, 2021, **21**, 1636.

52 A. Bondi, van der Waals Volumes and Radii, *J. Phys. Chem.*, 1964, **68**, 441.

53 S. Alvarez, A cartography of the van der Waals territories, *Dalton Trans.*, 2013, **42**, 8617.

54 (*a*) A. D. Becke and K. E. Edgecombe, A simple measure of electron localization in atomic and molecular systems, *J. Phys. Chem.*, 1990, **92**, 5397; (*b*) B. Silvi and A. Savin, Classification of chemical bonds based on topological analysis of electron localization functions, *Nature*, 1994, **371**, 683; (*c*) A. Savin, R. Nesper, S. Wengert and T. F. Fässler, ELF: The Electron Localization Function, *Angew. Chem., Int. Ed. Engl.*, 1997, **36**, 1808.

55 T. K. Meister, J. W. Kück, K. Riener, A. Pöthig, W. A. Herrmann and F. E. Kühn, Decoding catalytic activity of platinum carbene hydrosilylation catalysts, *J. Catal.*, 2016, **337**, 157.

56 (*a*) M. Parasram and V. Gevorgyan, Visible light-induced transition metal-catalyzed transformations: beyond conventional photosensitizers, *Chem. Soc. Rev.*, 2017, **46**, 6227; (*b*) K. P. S. Cheung, S. Sarkar and V. Gevorgyan, Visible Light-Induced Transition Metal Catalysis, *Chem. Rev.*, 2022, **122**, 1543.

57 F. Bonati and G. Minghetti, New isocyanide complexes of platinum(II), *J. Org. Chem.*, 1970, **24**, 251.

58 M. A. Kinzhalov, M. V. Kashina, A. S. Mikherdov, S. A. Katkova and V. V. Suslonov, Synthesis of Platinum(II) Phoshine Isocyanide Complexes and Study of Their Stability in Isomerization and Ligand Disproportionation Reactions, *Russ. J. Gen. Chem.*, 2018, **88**, 1180.

59 G. M. Sheldrick, A short history of SHELX, *Acta Crystallogr., Sect. A: Found. Crystallogr.*, 2008, **64**, 112.

60 O. V. Dolomanov, L. J. Bourhis, R. J. Gildea, J. A. K. Howard and H. Puschmann, OLEX2: a complete structure solution, refinement and analysis program, *J. Appl. Crystallogr.*, 2008, **42**, 339.

61 *Agilent, C., CrysAlis PRO*, Agilent Technologies Ltd, Yarnton, UK, 2014.

62 (*a*) J. P. Perdew, K. Burke and M. Ernzerhof, Generalized gradient approximation made simple, *Phys. Rev. Lett.*, 1996, **77**, 3865; (*b*) C. Adamo and V. Barone, Toward reliable density functional methods without adjustable parameters: The PBE0 model, *J. Chem. Phys.*, 1999, **110**, 6158.

63 (*a*) S. Grimme, S. Ehrlich and L. Goerigk, Effect of the damping function in dispersion corrected density functional theory, *J. Comput. Chem.*, 2011, **32**, 1456; (*b*) S. Grimme, A. Jens, S. Ehrlich and H. Krieg, A consistent and accurate ab initio parametrization of density functional dispersion correction (DFT-D) for the 94 elements H-Pu, *J. Chem. Phys.*, 2010, **132**, 154104.

64 (*a*) F. Neese, The ORCA program system, *Wiley Interdiscip. Rev.: Comput. Mol. Sci.*, 2012, **2**, 73; (*b*) F. Neese, Software update: the ORCA program system, version 4.0, *Wiley Interdiscip. Rev.: Comput. Mol. Sci.*, 2018, **8**, e1327.

65 F. Weigend and R. Ahlrichs, Balanced basis sets of split valence, triple zeta valence and quadruple zeta valence quality for H to Rn: Design and assessment of accuracy, *Phys. Chem. Chem. Phys.*, 2005, **7**, 3297.

66 J. D. Rolfes, F. Neese and D. A. Pantazis, All-electron scalar relativistic basis sets for the elements Rb–Xe, *J. Comput. Chem.*, 2020, **41**, 1842.

67 F. Neese, An improvement of the resolution of the identity approximation for the formation of the Coulomb matrix, *J. Comput. Chem.*, 2003, **24**, 1740.

68 D. A. Pantazis and F. Neese, All-Electron Scalar Relativistic Basis Sets for the Actinides, *J. Chem. Theory Comput.*, 2011, **7**, 677.

69 V. Barone and M. Cossi, Quantum Calculation of Molecular Energies and Energy Gradients in Solution by a Conductor Solvent Model, *J. Phys. Chem. A*, 1998, **102**, 1995.

70 (*a*) T. A. Keith, *AIMAll (Version 19.02.13)*, TK Gristmill Software, Overland Park KS, 2019; (*b*) T. Lu and F. Chen, Multiwfn: A multifunctional wavefunction analyzer, *J. Comput. Chem.*, 2012, **33**, 580; (*c*) T. Lu and F. Chen, Quantitative analysis of molecular surface based on improved Marching Tetrahedra algorithm, *J. Mol. Graphics Modell.*, 2012, **38**, 314.

71 W. Humphrey, A. Dalke and K. Schulten, VMD: Visual molecular dynamics, *J. Mol. Graphics Modell.*, 1996, **14**, 33.

72 J.-D. Chai and M. Head-Gordon, Long-range corrected hybrid density functionals with damped atom–atom dispersion corrections, *Phys. Chem. Chem. Phys.*, 2008, **10**, 6615.

73 M. J. Frisch, G. W. Trucks, H. B. Schlegel, G. E. Scuseria, M. A. Robb, J. R. Cheeseman, G. Scalmani, V. Barone, B. Mennucci, G. A. Petersson, H. Nakatsuji, M. Caricato, X. Li, H. P. Hratchian, A. F. Izmaylov, J. Bloino, G. Zheng, J. L. Sonnenberg, M. Hada, M. Ehara, K. Toyota, R. Fukuda, J. Hasegawa, M. Ishida, T. Nakajima, Y. Honda, O. Kitao, H. Nakai and T. Vreven, Gaussian 09, Revision B.01; Gaussian, Inc.: Wallingford, CT, USA, 2010.

74 D. Andrae, U. Häußermann, M. Dolg, H. Stoll and H. Preuß, Energy-adjustedab initio pseudopotentials for the second and third row transition elements, *Theor. Chim. Acta*, 1990, **77**, 123.

75 T. Lu and F. Chen, Multiwfn: A multifunctional wavefunction analyzer, *J. Comput. Chem.*, 2012, **33**, 580.

76 (*a*) M. J. Turner, J. J. McKinnon, S. K. Wolff, D. J. Grimwood, P. R. Spackman, D. Jayatilaka and M. A. Spackman, *CrystalExplorer17*, University of Western Australia, Perth, Australia, 2017; (*b*) P. R. Spackman, M. J. Turner, J. J. McKinnon, S. K. Wolff, D. J. Grimwood, D. Jayatilaka and M. A. Spackman, CrystalExplorer: a program for Hirshfeld surface analysis, visualization and quantitative analysis of molecular crystals, *J. Appl. Crystallogr.*, 2021, **54**, 1006.

77 J. J. McKinnon, D. Jayatilaka and M. A. Spackman, Towards quantitative analysis of intermolecular interactions with Hirshfeld surfaces, *Chem. Commun.*, 2007, 3814.
78 S. Sueki and Y. Kuninobu, Rhodium-catalysed synthesis of multi-substituted silylindenes from aryl alkynes and hydrosilanes via C–H bond activation, *Chem. Commun.*, 2015, **51**, 7685.
79 M. Pérez, L. J. Hounjet, C. B. Caputo, R. Dobrovetsky and D. W. Stephan, Olefin Isomerization and Hydrosilylation Catalysis by Lewis Acidic Organofluorophosphonium Salts, *J. Am. Chem. Soc.*, 2013, **135**, 18308.
80 F. E. Hahn and M. C. Jahnke, Heterocyclic Carbenes: Synthesis and Coordination Chemistry, *Angew. Chem. Int. Ed.*, 2008, **47**, 3122–3172.
81 M. A. Kinzhalov, A. A. Zolotarev and V. P. Boyarskiy, Crystal structure of *cis*-[$PdCl_2(CNMes)_2$], *J. Struct. Chem.*, 2016, **57**, 822–825.